Carbon and Strontium Isotope Chemostratigraphy of the Neoproterozoic Carbonates from the Amadeus Basin, NT

Thesis submitted in accordance with the requirements of the University of Adelaide for an Honours Degree in Geology

By Hamza Sulaiman Al Khanjari

November 2018

THE UNIVERSITY of ADELAIDE

CARBON AND STRONTIUM ISOTOPE CHEMOSTRATIGRAPHY OF THE NEOPROTEROZOIC CARBONATES FROM THE AMADEUS BASIN, NT

RUNNING TITLE
ISOTOPE CHEMOSTRATIGRAPY OF NEOPROTEROZOIC CARBONATES FROM THE AMADEUS BASIN

ABSTRACT

Stratigraphic sections that include Bitter Spring Group, Wallara Formation and Ringwood Member were selected from two cores in the Amadeus Basin, which are BR05DD01 and Wallara-1 to be examined, and evaluated using stable carbon isotopes (δ^{13}Ccarb) and radiogenic strontium ($^{87}Sr/^{86}Sr$) isotopes, together with major and trace elements, measured in carbonates. Correlation of acquired $\delta^{13}C$ and $^{87}Sr/^{86}Sr$ data with local and global C and Sr isotope records were explored and evaluated, and our results suggest that $\delta^{13}C_{carb}$ trend from studied cores showed strong correlation with presumably coeval global $\delta^{13}C$ records, however most of our $^{87}Sr/^{86}Sr$ data appeared to be more radiogenic than global marine Sr isotope record. This in turn suggests that the depositional environment of the Amadeus Basin was predominantly restricted with respect to a coeval Neoproterozoic open ocean. Also, this proposed basin restriction became more enhanced with time (from Tonian to Cryogenian/Ediacaran), however some $^{87}Sr/^{86}Sr$ data from Tonian's Bitter Spring Group are very close to expected global marine Sr isotope trend. This on the other hand is not the case for younger (Cryogenian, Ediacaran) carbonates from Amadeus Basin (e.g., Ringwood Member, Olympic Fm.) as these have systematically much more radiogenic $^{87}Sr/^{86}Sr$ signatures compared to the expected Neoproterozoic paleo-seawater 87Sr/86Sr trend. We also found high abundance of rubidium (Rb) in studied carbonate rocks, which will cause higher production of radiogenic strontium (^{87}Sr) within the bulk carbonates since their deposition. All our $^{87}Sr/^{86}Sr$ data were thus corrected for in-situ ^{87}Rb decay, which caused the measured strontium isotopes to be additionally more radiogenic. Nevertheless, even after this correction for Rb decay, our $^{87}Sr/^{86}Sr$ trends from most of studied carbonates are systematically more radiogenic than the global marine $^{87}Sr/^{86}Sr$ trend, further corroborating the above progressive restriction of the Amadeus Basin throughout the Neoproterozoic. Furthermore, based on C isotope constraints, we also argue that the formation carbonates in the top part of the BR05DD01 core corresponds to proposed the Aralka Formation, and its carbonate-rich Ringwood Member. The paleo-redox conditions were constrained using rare earth element (REE) patterns, specifically based on Ce anomaly (Ce/Ce*), where most of the results from studied Neoproterozoic carbonates showed positive Ce anomaly. This in turn indicate that the seawater/local basin waters in the Amadeus Basin were predominantly anoxic during the deposition of both Bitter Spring Group (Tonian) and Ringwood member (Cryogenian). However, selected carbonates from Bitter Spring Group sampled from Wallara-1 core showed true negative Ce anomaly, and also have less radiogenic $^{87}Sr/^{86}Sr$ values (close to expected global ocean) which thus might suggest a transient more oxic shallow-water conditions in marine dominated evaporitic settings, compared to rest of the studied Neoproterozoic carbonate records from the Amadeus Basin.

KEYWORDS

Amadeus Basin, Neoproterozoic, Carbon, Strontium, Isotopes, REE, Stratigraphy, Chemostratigraphy, Paleo-Redox

TABLE OF CONTENTS

LIST OF FIGURES

1. INTRODUCTION

The stratigraphy and intra-basin correlation of Neoproterozoic sedimentary successions in the Amadeus Basin are debatable, and many researchers have proposed different interpretations to resolve these problems using various methods (see Prichard and Quinlan, 1960, Normington and Edgoose 2018, Plummer 2018, and references therein). Prichard and Quinlan (1960) were among the first researchers who systematically investigated the Neoproterozoic stratigraphy of the Amadeus Basin, and proposed four different formations (Fm.) which are Bitter Springs Fm (oldest), Areyonga Fm, Pertatataka Fm and Arumbera Greywacke (youngest). Plummer (2018) and Normington (2018) presented the most recent revision of the stratigraphy recently, where the interpretations have been revised based on seismic lithological and HyLoggerTM data. In addition, Verdel and Cambell (2017) generated a composite C isotope record of Neoproterozoic carbonates from the NE parts of the basin. The above studies thus generated a revised stratigraphy and correlations of Neoproterozoic sequences within the Amadeus Basin, however, one of the open and remaining questions was the correlation and chronostratigraphy of two drill cores (BR05DD01 and Wallara-1), as discussed in Plummer (2018). These cores should presumably record the following sequence of Neoproterozoic successions (ordered from oldest to youngest): Heavitree / Dean Quartzite, Bitter Springs Group, Wallara Fm, Areyonga Fm, Aralka Fm, Olympic Fm / Pioneer Sandstone, Pertatataka Fm, Carnegie Fm (for details see also Fig.1). The primary focus of this thesis is to use isotope chemostratigraphy as a tool to further test and better constrain the above proposed stratigraphy and correlations of Neoproterozoic (Cryogenian) sequences in the Amadeus Basin (see Fig. 1). In particular, this study investigates carbon (C) and strontium (Sr) isotopes, as well as elemental concentrations (including REE), in

carbonates from the above two drill cores, and the acquired isotope trends are then compared to existing and published C and Sr isotope data from other parts of Amadeus Basin (Verdel and Campbell 2017, Phelps 2015), as well as to the global marine C and Sr isotope trends over Neoproterozoic (Halverson et al. 2007, Cox et al. 2016).

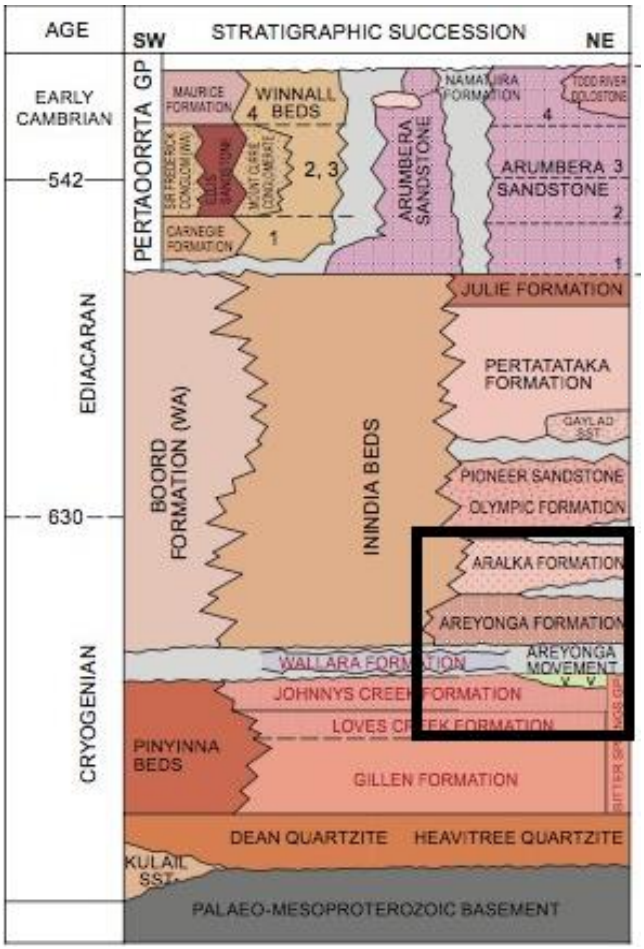

Figure 1: The stratigraphy of the Neoproterozoic and Early Cambrian, which is adapted from NTGS (Normington et al., in review). The black box shows the interval studied in this project starting from Loves Creek Formation and ending with the Aralka Formation.

The principles of isotope chemostratigraphy techniques, which have become common and more popular since about 1980, is to characterize the carbonate depositional units for correlation purposes by relying on similarities (or differences) in isotope and geochemical traits and their stratigraphic variation among different carbonate sequences (Ramkumar, 2015). This project thus aims to generate a detail C and Sr isotope and chemo-stratigraphic record for the Neoproterozoic successions in the

Amadeus Basin (BR05DD01 located to the west, and Wallara-1 located 180 Km east from BR05DD01, Figure 2); and to correlate these records to the local and/or global Neoproterozoic isotope trends.

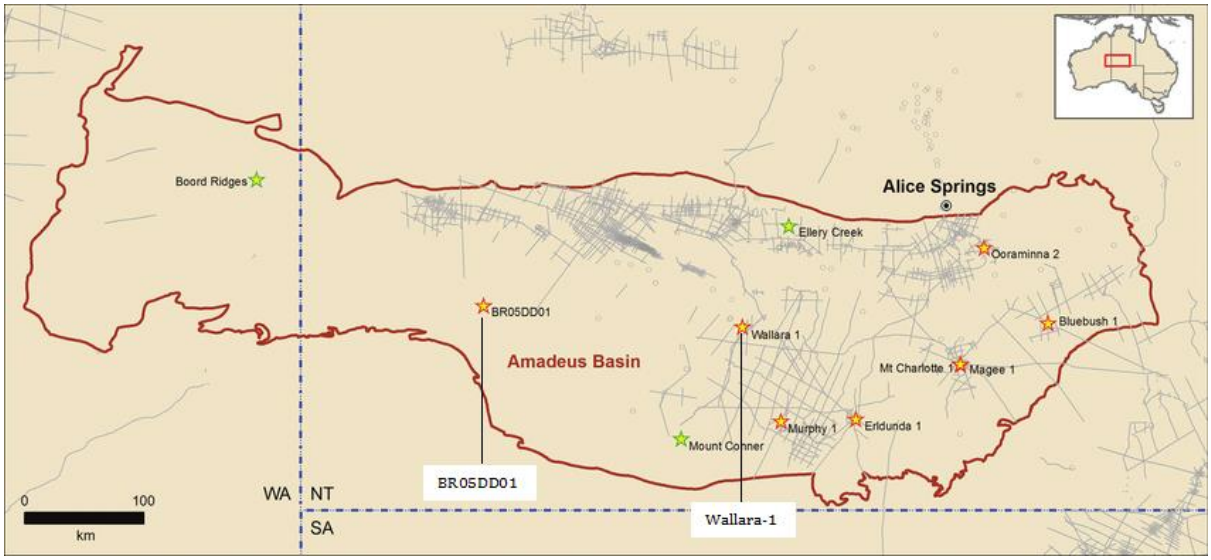

Figure 2: Map that shows the two studied drill cores (BR05DD01 and Wallara-1) with their locations in the Amadeus Basin in central Australia adapted from Plummer (2018).

One of the major issues that previous studied raised (see Plummer, 2018) while constructing the Neoproterozoic stratigraphy of BR05DD01 core is defining the formation between 500-200 m in depth, where previous studies suggested this to be the Pertatataka Formation (Ambrose et al. 2010) and assumed an unconformity in this depth; while others suggest that it is the Aralka Formation (including its carbonate-rich Ringwood Member) and that there is no unconformity (see Plummer, 2018; Normington and Edgoose, 2018). This study aims to resolve this issue by correlating $\delta^{13}C_{carb}$ data acquired from BR05DD01 core with available C isotope data from northeast parts of the Amadeus Basin (i.e., Limbla Syncline, see Verdel and Campbell, 2017) and/or global C isotope trends. In the Neoproterozoic, the presumably global marine C isotope records throughout the Ediacaran and Cryogenian (based on data from sedimentary carbonates in Canada, Uruguay, Siberia,

Norway, Namibia, southern China, Brazil, Australia and Oman) show systematic temporal changes with numerous positive and negative C isotope excursions, where some of these reached values lower than the composition of a "canonical" mantle ($\delta^{13}C \approx -5‰$), (Ramkumar, 2015, Halverson et al. 2007, Cox et al. 2016).

This project thus also aims to link the local carbon isotope variation in the Neoproterozoic carbonates from the Amadeus basin to well-documented global $\delta^{13}C$ marine record, using carbonate/dolomite samples from the formations shown in Figure (1). Another chemostratigraphy method that is useful for indirect "dating" of marine carbonates is based on the radiogenic strontium isotopes ($^{87}Sr/^{86}Sr$ ratios) and so-called Strontium Isotope Stratigraphy (SIS) technique (McArthur et al. 2012; Kuznetsov et al., 2018 and reference therein), which is also used in this project for selected depths that contains high carbonate abundances from the formation studied. The SIS technique depends on the fact that the signature of $^{87}Sr/^{86}Sr$ on the ancient and modern global ocean is anticipated to be isotopically homogenous because the residence time of Sr in the ocean is much longer (ca. 1 million years) compared to typical mixing time of the global ocean (ca. 1000 years), (see McArthur et al. 2012). The modern seawater budget of Sr isotopes is primarily controlled by two main Sr input fluxes, which are hydrothermal inputs (with $^{87}Sr/^{86}Sr$ of ~0.703) and weathering of continental crust (~0.716; Edwards et al., 2015). Therefore, temporal changes in oceanic $^{87}Sr/^{86}Sr$ signature over geological time are mainly a function of changing magnitudes of the above Sr fluxes, which in turn are controlled by planet's tectonic history (Kuznetsov et al., 2018; Love, 2017 and references therein).

As to the Neoproterozoic era, the $^{87}Sr/^{86}Sr$ trend of paleo-seawater increased systematically from Tonian to Eiacaran/Cambrian (Cox et al., 2016) most likely due

to the rapid continental crust weathering linked to the origin of Pan-African Orogen System and the assemblage of Gondwana (Kuznetsov et al., 2018).

2. BACKGROUND

2.1. Geological Setting

The Amadeus Basin is located in central Australia and is shared by two states NT and WA, i.e., Northern Territory and Western Australia. The Amadeus Basin covers an area of approximately 170,000 Km^2 and consist of variegated and thick Neoproterozoic to early Palaeozoic succession, which includes carbonate, evaporate and clastic sedimentary rocks (Plummer, 2018). The Amadeus Basin geology consist of two packages that are separated by unconformities; (1) sedimentary rocks that are Cambrian to Carboniferous in age, and (2) glacial and sedimentary rocks from the Neoproterozoic era (Schmid, 2017, Verdel and Campbell, 2017). Post depositional salt tectonics have been the main control in the present structural framework related to two major orogenies, which are Alice Springs (450-300 Ma) and the Petermann Orogeny (570-530 Ma), resulting in the compression in general NNE-SSW direction (Schmid, 2017). The accumulations of the Neoproterozoic sedimentary successions in the Amadeus Basin reach an average thickness of about 3-4 Km (Verdel & Campbell, 2017), however at some locations of main depocenters in the burial depths in the basin reach up to ~7 Km (Schmid et al., 2016). The sections below describe main Formations/Members and Groups of Neoproterozoic sedimentary sequences recognized throughout the Amadeus Basin (Normington and Edgoose 2018; Plummer 2018; Verdel and

Campbell, 2017), and these are also the main target rocks for this project and isotope chemostratigraphy studies.

2.2. Ringwood Member

The carbonate rich Ringwood Member is part of the Cryogenian Aralka Formation and the Member is described as limestone and/or dolostone, pisolitic and stromatolitic carbonate which are apparent in some parts, and it has infrequent breccia, insignificant siltstone and exhibits calcarenite (Wells et al., 1967). The Member comprises four sub members or units which are: (1) basal carbonate conformably positioned on Areyonga Formation glacial deposits, thin bedded carbonate is also placed on top of this carbonate basal; (2) interval that is rich in carbonate and categorized by stromatolite that is domical; (3) superimposing the para-sequences of carbonate linked below and above by intervals of stromatolite (4) laminated carbonate and siltstone make up the upper part (Verdel & Campbell, 2017). All the Ringwood Member parts are exposed well in the north eastern region of Amadeus Basin in the syncline of Limbla, and only parts (1) and (2) are well exposed in the whole Amadeus Basin (Verdel & Campbell, 2017. but see also Normington and Edgoose 2018).

2.3. Pertatataka Formation and Associated Sedimentary Sequences

The Ediacaran/Cryogenian Pertatataka Formation was redefined from Madigan's (1932) by Prichard and Quinlan (1960), where they described it as clastic sequence with fine grains that conformably sets amongst the Arumbera Greywacke that overlies it and the Areyonga Formation that sets beneath it. The Formation was later redefined and divided regionally to four parts which are now recognized as: (1) a lower unit that consists mainly of fine grey to black clastics

(Aralka Formation) placed conformably above the Areyonga Formation; (2) coarse clastic succession that disconformably sets above the previous part which comprises of diamictites, sandstones and conglomerates, which normally has a dolostone cap (Olympic Formation); (3) Mostly green and red clastics that has fine to medium grains (Pertatataka Formation) and overlies the prior unit; and finally (4) the upper part contain dolostones and limestones (Julie Formation) which sets conformably beneath the Arumbera Sandstone (based on Preiss et al, 1978, Plummer, 2018).

2.4. Bitter Springs Group

The Tonian Bitter Springs Group stratigraphy consists of three formations, which are Gillen Formation, Loves Creek Formation and Johnnys Creek Formation ordered form oldest to youngest. This study will not cover Gillen Formation, but will focus on the other two formations.

2.4.1. LOVES CREEK FORMATION

The formation was described by Southgate (1989) as cyclic and stromatolitic dolostone sequence, which continues laterally in the interval with typical thicknesses between 2 and 12 meters, its stromatolites develop in stratiform, tabulate, columnar and domal shapes relying on the depth of water it grows in (Southgate, 1989). These stromatolite assemblages also contain distinct Acaciella australica species which through Australia produce a marker horizon (Walter, 1972). The environment of deposition for this formation was interpreted by Oehler et al., (1979) as shallow and open marine environment and then was redefined by Southgate (1989) as rapid transgressive accumulations at the base and are overlain by cycles that are shallowing upward.

2.4.2. JHONNYS CREEK FORMATION

The Jhonnys Creek Formation comprises of siltstone that has also evaporitic components and the formation is mainly red in color, and contains also shales with greyish limestone and yellowish to greyish dolostones (Schmid et al., 2016). The maximum thickness of the Jhonnys Creek Formation with the partially cherty carbonates reach up to 35 meter (Schmid et al., 2016). The Formation is commonly seperated by erosional contacts that are indurate to karstic or gradational margins of red siltstone (Schmid et al., 2016). The Formation has many evaporitic depositional environment features, such as cracks associated to desiccation and pseudo morphs caused by halite (Schmid, 2017), along with abundant carbonates divided into stromatolitic, dolomitic limestone and laminated to thin bedded dolostone (Southgate, 1986, Schmid, 2017).

2.5. Neoproterozoic $\delta^{13}C_{carb}$ Record in the Amadeus Basin

Available $\delta^{13}C_{carb}$ data of the Neoproterozoic carbonate sequences in the Amadeus Basin were compiled and published recently by Verdel and Campbell (2017), where they measured C isotopes in sections exposed in the northeastern parts of the Amadeus Basin to produce a composite $\delta^{13}C_{carb}$ record based on the Tonian, Cryogenian and the Ediacaran carbonates (i.e., Bitter Springs Gr., Ringwood Mb., and Olympic and Julie Fms.). This record is shown in Figure (3) illustrating negative excursion in the Bitter Spring Group (about -8%) that might be associated with changes in the marine C cycle that occurred to the global environment, and another systematic negative excursion was found in the Ringwood Member, and finally the Olympic Formation conserve a similar negative excursion linked to the aftermath of the Marionaon glaciation (Verdel and Campbell, 2017).

The above study correlated the composite C isotope record from the Amadeus Basin to other coeval carbonate records from around the world, and data indicate that the excursions match quite well other Cryogenian records found in Scotland-Ireland, North-West of Canada, the Death Valley area in South-West of the United States. Stratigraphic equivalents of the upper Ringwood Member from the eastern Amadeus Basin stromatolites was found in Balcanoona Formation in Adelaide rift complex (Verdel and Campbell, 2017). Overall, the C isotope record from the Amadeus can be also correlated to the Cryogenian/Ediacaran carbonates from Namibia, Mongolia as well as the Tapley Hill Formation (in Adelaide rift complex, Verdel and Campbell, 2017).

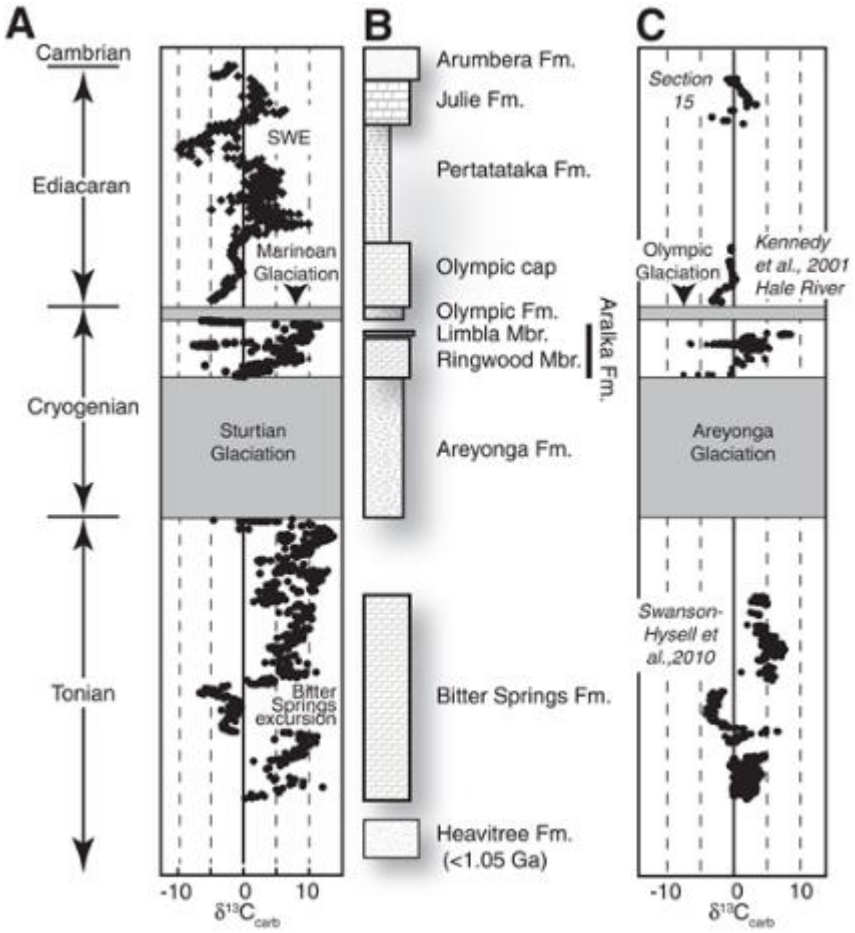

Figure 3: (A) Global marine $\delta^{13}C_{carb}$ record of Neoproterozoic carbonates (adapted from Halverson et al., 2005; Macdonald et al., 2009) compared to $\delta^{13}C_{carb}$ record of the Amadeus Basin (C), where data come from Verdel and Campbell (2017), Kennedy et al. (2001), and Swanson-Hysell et al. (2010). Gaps in (B) shows unconformities and/or lack of carbonate deposition in the Amadeus Basin.

2.6. Strontium Isotope ($^{87}Sr/^{86}Sr$) Record in the Neoproterozoic Carbonates

Composite Sr isotope strontium record of Neoproterozoic marine carbonates from multiple locations world-wide was published by Halverson et al. 2007 and revised recently by Cox et al. (2016), where they pre-screened the carbonate samples for the diagenesis based on Sr, Mn/Sr, Mg/Ca data, as well as Rb concentrations. Commonly, prior to elemental and Sr isotope analysis of carbonates these were leached in ammonium acetate, then washed in MQH_2O to rinse exchangeable cations attached to clays and other non-carbonate componentsit, and finally

leached in weak acid for TIMS analysis (see Halverson et al., 2007 and references therein). This composite paleo-seawater $^{87}Sr/^{86}Sr$ record for the Neoproterozoic era is shown in Figure 4 (from Cox et al., 2016; source data from Halverson et al. 2007, 2010).

As it illustrated in Figure (4) during the early Neoproterozoic (Tonian) there is $^{87}Sr/^{86}Sr$ trough or stable plateau that overlaps with the interval of 950-850 Ma that is associated with the break-up of Rodinia and possible initiations of Mozambique Ocean or exposure of larger basaltic igneous provinces (Cox et al., 2016;). Then, about 850-840 Ma, the marine Sr isotope record increases abruptly to values > 0.7060 before the drop in 830Ma to a value of 0.7055, which is likely caused by the Guibei and Willouran LIP's emplacement (Cox et al., 2016). Prior to the onset of glaciation onset in the Cryogenian there was a drop in $^{87}Sr/^{86}Sr$ from 0.7070 to 0.7064, then throughout the Cryogenian $^{87}Sr/^{86}Sr$ rises abruptly to a stable values of ~0.7073. This drop in Sr isotope record that occurred prior to the Cryogenian is observed in carbonate records from East Greenland, Svalbard and Mackenzie Mountains of North-West Canada in the Coates Lake Group (Cox et al., 2016).

The strontium isotope record published for the Neoproterozoic carbonates from Australia and the Amadeus Basin (Phelps, 2015) reveals generally more radiogenic values (Figure 5) than the global Neoproterozoic seawater $^{87}Sr/^{86}Sr$ trend (Figure 4, data from Cox et al., 2016). These generally more radiogenic $^{87}Sr/^{86}Sr$ values in the Neoproterozoic carbonates from Australia are possibly explained by three processes, which are: (1) the signatures of $^{87}Sr/^{86}Sr$ in bulk carbonate are contaminated by clays, (2) the Neoproterozoic carbonate of

Australia might be deposited in marine environment that is more restricted and effected by local inputs from continental weathering supplying more radiogenic Strontium, and/or (3) by diagenesis and the impact of meteoric fluids causing resetting of primary marine Sr isotope data (Banner and Hanson, 1990; Kennedy, 1996).

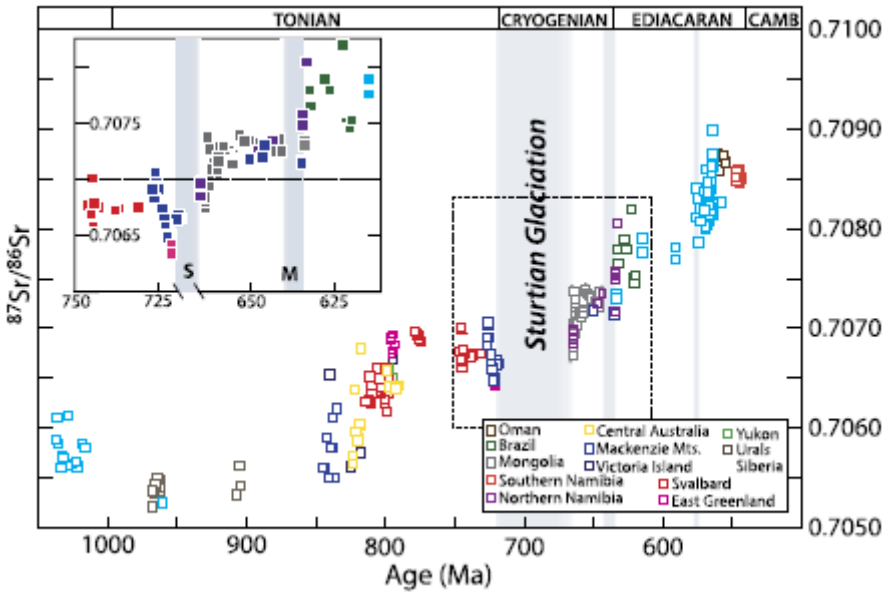

Figure 4: Global Neoproterozoic seawater $^{87}Sr/^{86}Sr$ record by Cox et al. (2016), which has been revised from (Halverson et al. 2007, 2010) previous records and combined with other previous data published.

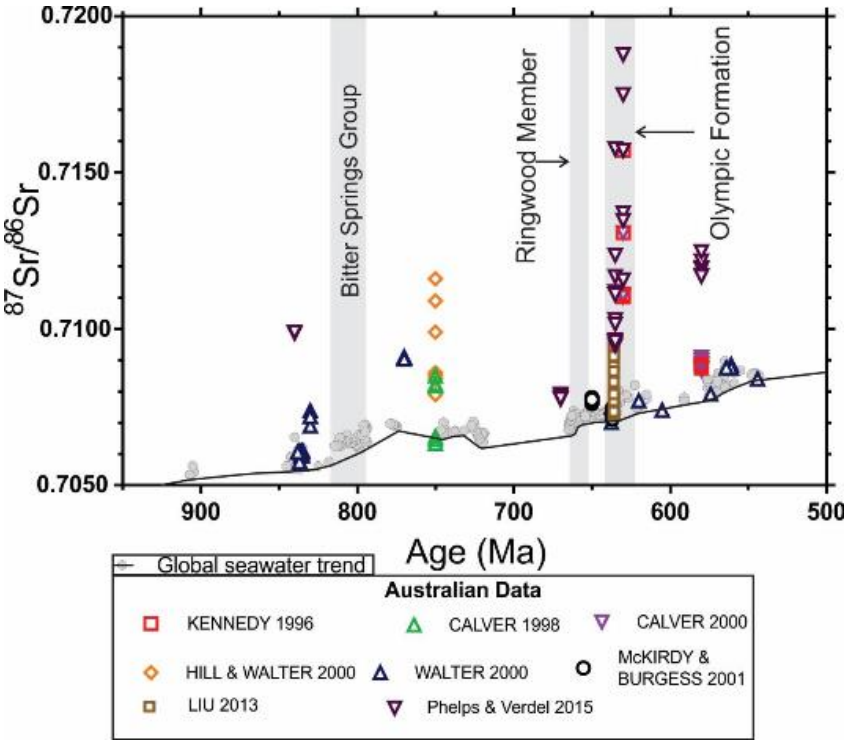

Figure 5: Global Neoproterozoic seawater 87Sr/86Sr records by Cox et al. (2016), and additional data from Australian regions including the Amadeus Basin by Kennedy (1996) and Phelps (2015), from Togari Group and Tasmania by Calver (1998), from Upper Burra Group by Hill_ Walter (2000), from Bitter Springs Group in Amadeus Basin and Adelaide Rift Complex by Walter (2000), from the Upper Burra Group in Adelaide Rift Complex by Calver (2000), from Brighton Limestone in the Etina Formation by Mckirdy_Burgess (2001), from the Nuccalena Formation in Adelaide Rift Complex by Liu (2013).

3. METHODS

3.1. Sample Collection

Carbonate rich samples of BR05DD01 core were collected from Northern Territory Geological Survey (NTGS) core library in Alice Springs in NT (central Australia). A total of 358 dolomite-rich samples were chosen from the core (using also HyLogger Data as guide) starting from the depth of 1193.3 meters and ending with the depth of 155.7 meters. Shale samples were avoided and dolomite samples were collected for every two meters; except for the Aralka Formation (484.44–155.7 m), where samples were collected after generally every meter from the interval of interest (~160 to 170 meters). Dolomite samples from Wallara-1 core were provided for this project by a former PhD student from the University

of Adelaide (Dr. Robert Klaebe), and these samples cover the depth interval from 1929.40m to 1967.50m (see Klaebe 2016)

3.2. Samples Preparation: Drilling, Leaching, and Stable Isotope Analysis

A total of 223 samples were selected and drilled from all depths covered in BR05DD01 core. A powder volumes corresponding to about a third to half volume of 2 ml centrifuge tube was drilled and collected for each sample. Subsequently, an amount of 5 mg of each sample was weighted and separated to another 2 ml centrifuge tube and sent to Canada (McGill University) for $\delta^{13}C_{carb}$ and $\delta^{18}O_{carb}$ analyses using conventional IR MS (for details see also method described in Halverson et al. 2010). These samples were then reduced to 78 samples that yielded the most carbonate-rich bulk samples, which includes Loves Creek Formation, Wallara Formation and Ringwood member. Furthermore, 40 samples from BR05DD01 core were selected for Sr isotope analysis ($^{87}Sr/^{86}Sr$ ratios) done by TIMS at the University of Adelaide, where 10 samples came from the Ringwood Member and the other 30 from the Bitter Spring Group. All the above samples used for Sr isotope analysis were also analysed for elemental concentrations at Adelaide Microscopy Centre (Uni. Adelaide) using ICP MS. Finally, additional 20 samples from the Loves Creek Formation were selected as well for Sr isotope analysis from the Wallara-1 core.

The above carbonate samples from BR05DD01 and Wallara-1 cores, which were selected for elemental and Sr isotope analyses were leached prior to analysis to minimize the effect of possible clays contamination and the impact of detrital constituents on measured elemental (including REE) and radiogenic Sr isotope data. Specifically, the powder mass was documented before the leaching process

and after it, and the leaching procedure was done similarly as Love (2017), modified from Liu et al. (2014), where the samples were leached three times. The first step involved leaching (50-100 mg) of the powder in of 1M ammonium acetate that is ultra-pure for one hour, followed by sonication for 20 minutes and centrifuging for 10 minutes (4000 RPM).

This first leachate was discarded because it mostly has non-carbonate Sr that is linked with clay fraction positions that are interchangeable (Liu et al., 2014). The second step consisted of leaching with 0.2M acetic acid that is Ultra-pure at room temperature for one hour, then sonication for 20 minutes and centrifuging for 10 minutes (4000 RPM). The produced leachate was also discarded in order to decrease the effect of clay-related Sr fraction on measured $^{87}Sr/^{86}Sr$ values. Lastly, the samples were leached in 0.2M acetic acid that is Ultra-pure at room temperature for one hour, then sonicated for 20 minutes and centrifuged for 10 minutes (4000 RPM). The produced solutions which contain mainly Sr associated to carbonate phases were then placed in cleaned Teflon vials, which were subsequently dried down. These dry samples were placed in about 5ml of 2% suprapure nitric acid (HNO_3) to make it ready for the elemental concentrations analysis and Sr purification method done prior to TIMS analysis of Sr isotopes.

3.3. Analysis of Elemental of Concentrations by ICP MS

The aliquot of each sample that were digested using the nitric acid were made in two different dilutions, one at 1500-3000 times for trace elements and one at 100,000 times for major elements to be analysed by ICP MS at Adelaide Microscopy Center at the University of Adelaide, using the Inductively Coupled Plasma - Mass Spectrometer (ICP-MS Agilent 8900). The elemental

concentrations analytical error was typically about 2.5% , which was determined by measuring also a certified reference carbonate standard: (JDo-1 dolomite standard).

3.4. Eluent Chromatography and Sr Purification Method and Isotope Analysis by TIMS

Prior to TIMS analysis of Sr isotopes, the strontium have to be purified and separated from the sample matrix, using column chemistry based on Sr-Spec resin to get rid of Mg and Ca high contents in the samples, and other trace elements. For details on the method see Love (2017). The purified Strontium fractions were then loaded onto Re zone-refined filaments using Bircks solution. The filaments were then loaded to a multi-collector Phoenix TIMS instrument which made precise measurements of strontium isotope abundances, $^{87}Sr/^{86}Sr$ ratios, which were internally normalised (for more details see also Appendix B).

3.5. Correction of $^{87}Sr/^{86}Sr$ due to In-Situ ^{87}Rb Decay

Values of $^{87}Sr/^{86}Sr$ obtained from TIMS instrument were corrected due to in-situ ^{87}Rb decay from Rb present in the sample, which causes the ingrowth of radiogenic ^{87}Sr. The equation used for this correction was as follows (based on Nurgalieva et al., 2007):

$$(^{87}Sr/^{86}Sr)_0 = (^{87}Sr/^{86}Sr)_{meas.} - {}^{87}Rb/^{86}Sr \cdot (e^{\lambda t} - 1)$$

where $(^{87}Sr/^{86}Sr)_0$ is the corrected or primary Sr isotope ratio, $^{87}Rb/^{86}Sr$ is the measured ratio (derived from elemental Rb/Sr ratio analysed by ICP MS), and λ is the ^{87}Rb decay constant of $1.42 \cdot 10^{-11}$ yr^{-1}, and t is time in years, and finally

$(^{87}Sr/^{86}Sr)_{meas.}$ is the measured (uncorrected) Sr isotope ratio in a sample (Neumann & Huster, 1974; Nurgalieva et al., 2007).

4. RESULTS

4.1. $\delta^{13}C_{carb}$ and $\delta^{18}O_{carb}$ Data from Bulk Carbonates

Values of $\delta^{13}C_{carb}$ and $\delta^{18}O_{carb}$ were obtained for selected 78 Neoproterozoic dolomites samples from BR05DD01 that include Bitter Spring Group (Loves Creek Formation), Wallara Formation and the Ringwood Member. The following figures and discussions only comment on C isotope data, but O isotope ($\delta^{18}O_{carb}$ data) results from the above samples are available in the Appendix. C. As shown in Figure 6, the C isotope record (normalized to VPDB) of the Bitter Spring Group has negative $\delta^{13}C_{carb}$ excursion that increases with progressive depth, while Wallara Formation shows positive excursion overall, and Ringwood Member values varies from -2 to 3 per mil, and also showed noticeable negative $\delta^{13}C_{carb}$ excursion.

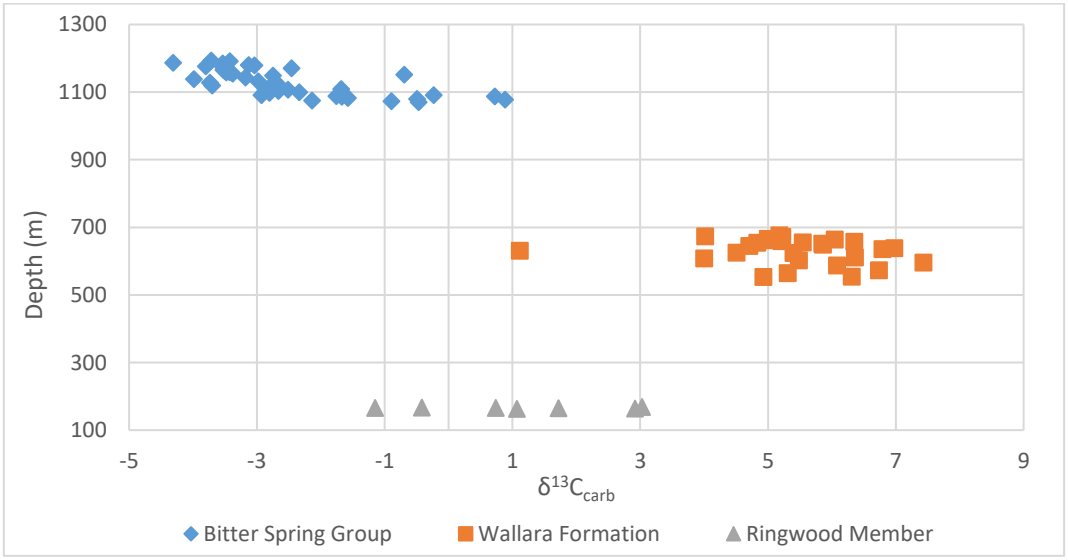

Figure 6: Measured $\delta^{13}C_{carb}$ (VPDB) data which comes from carbonates collected from BR05DD01 core , specifically, from three formations (Bitter Spring Group, Wallara Formation and Ringwood Member) plotted against the stratigraphic depth in meters in the X-axis.

4.2. Element Concentrations Data and Elemental Ratios

Concentrations of selected major and trace elements, including REE (see data in Appendix D) were measured for 40 samples from BR05DD01 core (30 from Loves Creek Formation and 10 Ringwood Member), and also 20 samples from Wallara-1 core (Loves Creek Formation). The selected elemental ratios (ppm/ppm) were then calculated and plotted as Al/Ca, Mn/Sr and Rb/Sr as indices for detrital clay contamination, meteoric diagenesis and the evaluation of in-situ rubidium (Rb) decay, respectively.

Figure 7 shows that strontium concentrations (ppm) are mostly less than 300 ppm for all studied carbonate. Moreover, Bitter Spring Group from Wallara-1 core had higher values for meteoric diagenesis indicator (Mn/Sr ratios) compared to BR05DD01 core, where Bitter Spring Group from BR05DD01 showed very low Mn/Sr values that are even lower than the Ringwood Member. Clay contamination (monitored via Al/Ca and Rb/Sr indices) apparently has high impact in all the studied formations from both cores with generally least affected Ringwood Member (relative to Bitter Spring Group samples). Finally, the Rb/Sr ratio showed high values in the Bitter Spring Group for both studied cores (BR05DD01 and Wallara-1), for details see data in Figure 7.

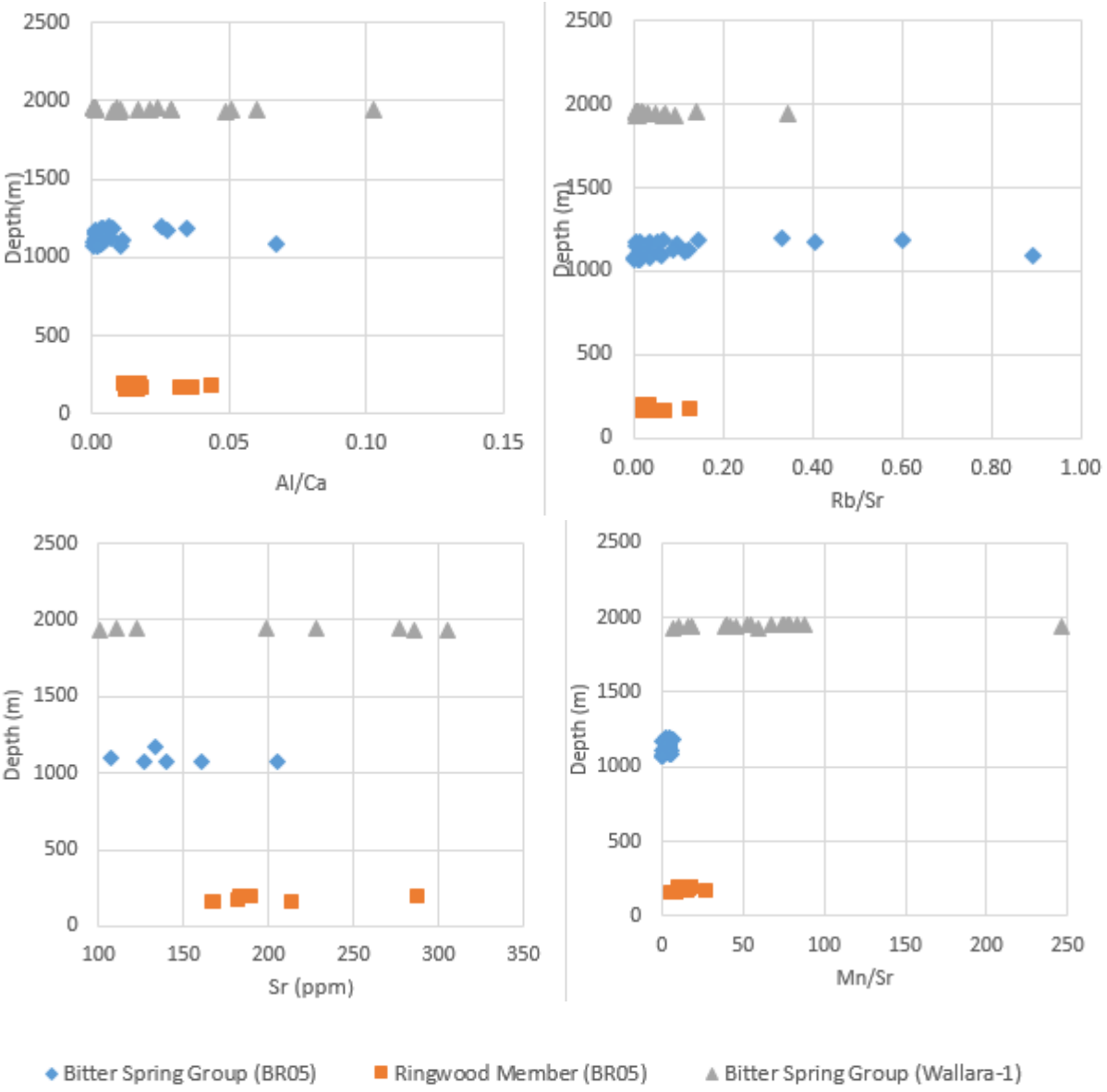

Figure 7: Sr isotope concentration and measured elemental ratios (Mn/Sr, Al/Ca and Rb/Sr) plotted against depth in meter for two formations (Bitter Spring Group and Ringwood Member), from two cores (BR05DD01 and Wallara-1).

4.3. Radiogenic $^{87}Sr/^{86}Sr$ Ratios Measured in Leached Carbonates

Values of $^{87}Sr/^{86}Sr$ for a total of 59 samples were obtained from both BR05DD01 (39 samples) and Wallara-1 cores (20 samples), which includes the Loves Creek Formation from both cores, and for the tested Ringwood Member samples were collected only from BR05DD01 core. These results were then corrected for in-

situ ^{87}Rb decay that causes ingrowth of radiogenic ^{87}Sr, which thus additionally shifts measured $^{87}Sr/^{86}Sr$ to more radiogenic values, obscuring the primary Sr isotope signature of carbonates and by inference that of paleo-seawater and/or local basin waters. These corrected $^{87}Sr/^{86}Sr$ results are plotted against their depths (Figure 8). Most of the $^{87}Sr/^{86}Sr$ values we obtained ranged between ~0.7066 and ~0.7200 with few exceptions in Bitter Spring Group that came from BR05DD01 core, where three values came to be more than 0.7200 which is possibly due to clay contamination.

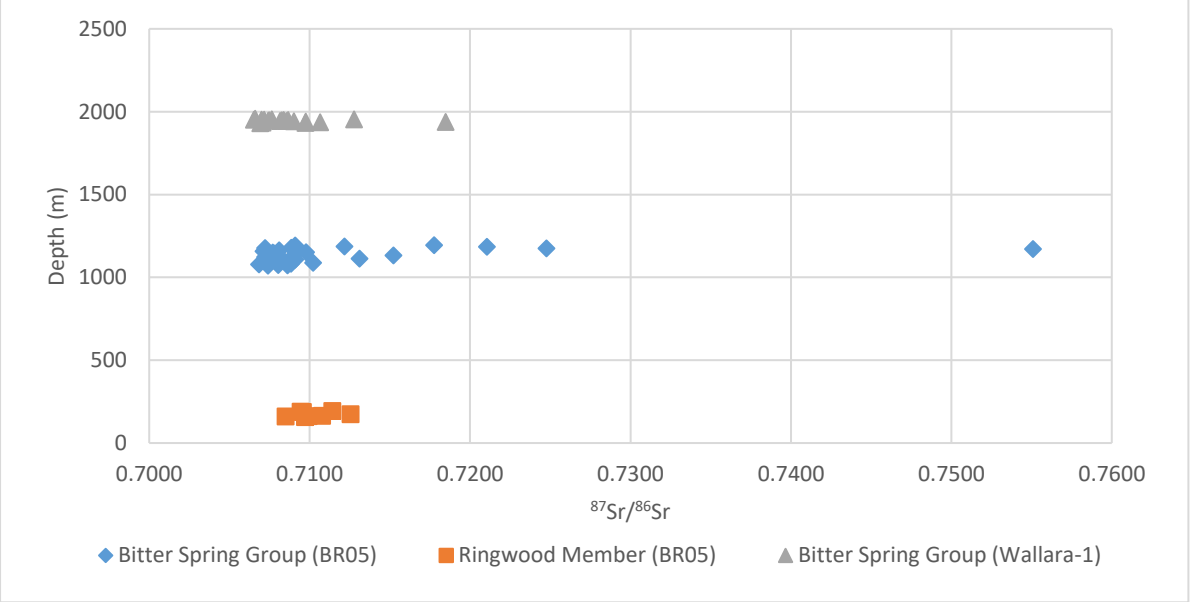

Figure 8: Corrected $^{87}Sr/^{86}Sr$ values (for in-situ ^{87}Rb decay) for two formations (Bitter Spring Group and Ringwood Member) from two cores (BR05DD01 and Wallara-1) plotted against depth in meters.

4.4. Rare Earth Elements and Ce/Ce* Anomaly Data : Paleo-Redox Proxy

Rare Earth Elements (REE) are very important in terms of providing past marine redox conditions based on analysis of marine carbonates (Tostevin, 2016). One of the most important redox sensitive REEs is Ce, which can be normalized (Ce/Ce*) and used as paleo-redox proxy using the following equation:

$$Ce/Ce* = [Ce/Ce_{(PAAS)}]/ 0.5\times(La/La_{(PAAS)}) + 0.5\times(Pr/Pr_{(PAAS)})$$

PAAS stands for Post-Archean Average Australien Shale (Taylor and McClennan, 1985). These calculated Ce/Ce* anomalies were then plotted against Pr normalized values (Pr/Pr*) which are measured and calculated using a very similar approach (as Ce anomalies) based on the following equation:

$$Pr/Pr* = [Pr/Pr_{(PAAS)}]/ 0.5\times(Ce/Ce_{(PAAS)}) + 0.5\times(Nd/Nd_{(PAAS)}).$$

The cross-plot of Ce/Ce* versus Pr/Pr*is then used to distinguish between true negative Ce anomaly (i.e., redox signal) and possible positive La anomaly that have no relationship to redox processes (see Figure 9). The results of Ce/Ce* anomalies shown in Figure 9 originate from 60 samples from the studied two cores, specifically 50 samples from Bitter Spring Group (Loves Creek Formation) and 10 samples from Ringwood Member. Most of the acquired Ce/Ce* anomaly data shown in figure 9 indicate that the Bitter Spring Formation and the Ringwood Member data plot in the middle between positive and negative Ce anomalies leaning more to the positive Ce anomaly for both cores studied. Moreover, few values from Wallara-1 core (Bitter Spring Group) exhibit true negative Ce anomalies, which suggest that the system was not entirely anoxic at that time, and redox conditions at this part of the basin were relatively more oxic, compared to rest of the records analysed in this study.

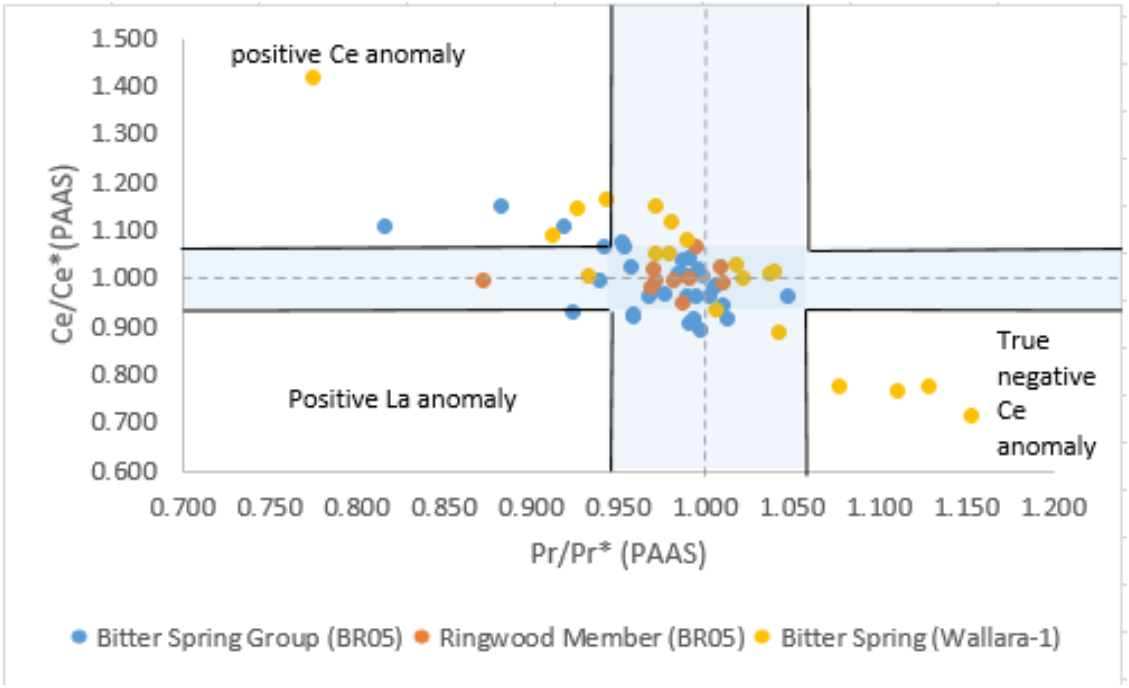

Figure 9: A cross plot of Ce/Ce*(PAAS) and Pr/Pr*(PAAS) anomalies (normalized to Post-Archean Average Australian Shale, PAAS), where data are from two Formations/Members: Loves Creek Formation and Ringwood Member, originating from two wells: BR05DD01 and Wallara-1.

5. DISCUSSION

5.1. Correlation of $\delta^{13}C_{carb}$ Data from BR05DD01 Core with Published C isotope Records from the Amadeus Basin

The composite $\delta^{13}C_{carb}$ record from the Amadeus Basin was presented recently in a study by Verdel and Campbell (2017) which is also discussed in detail in the section 2.5. This local C isotope record was plotted and compared to our $\delta^{13}C_{carb}$ data from BR05DD01 core (Figure 10a), where our data appears to be generally well correlated with this composite C isotope record of the Amadeus Basin, the latter constructed based on outcrop samples collected from the NE part of the basin (Verdel and Campbell, 2017). In particular, the $\delta^{13}C_{carb}$ data and trend from the purported Ringwood Member (from BR05DD01 core) appears to follow and overlap with the C isotope data published for this Member by Verdel and

Campbell (2017), where both our and published $\delta^{13}C_{carb}$ trends show a negative isotope anomaly with a magnitude of about 4 per mil (for details see data in Figure 10B and 10C). This agreement thus seems to confirm that the carbonate unit, and in general record between 500-200 m in the BR05DD01 core is indeed part of the Aralka Formation (with carbonate-rich Ringwood Member) and not the Pertatataka Formation, which agrees with the proposition of Normington and Edgoose (2018) and partly also with Plummer (2018) revised interpretations of the stratigraphy of BR05DD01 core.

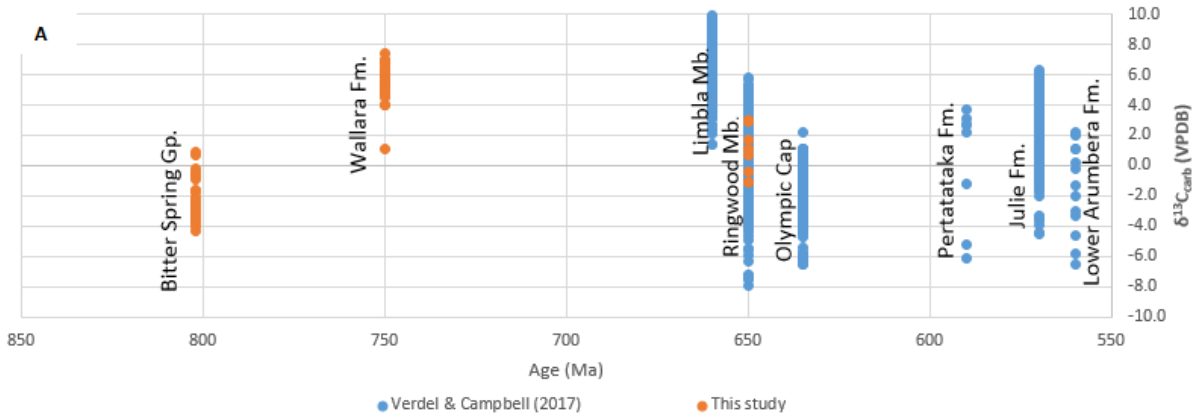

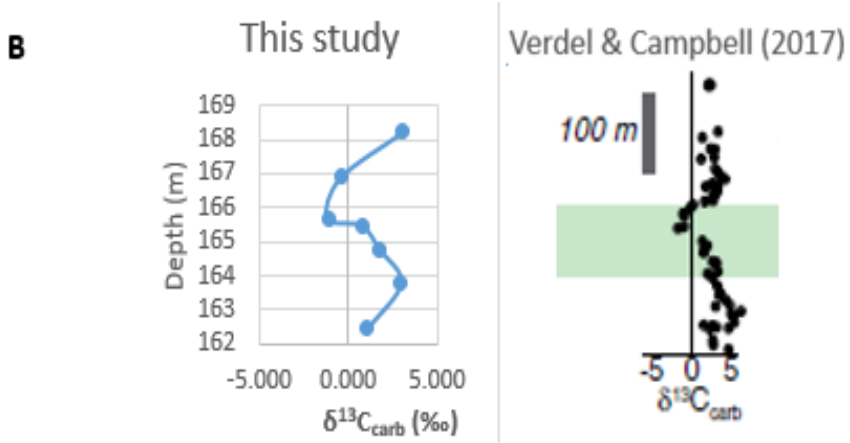

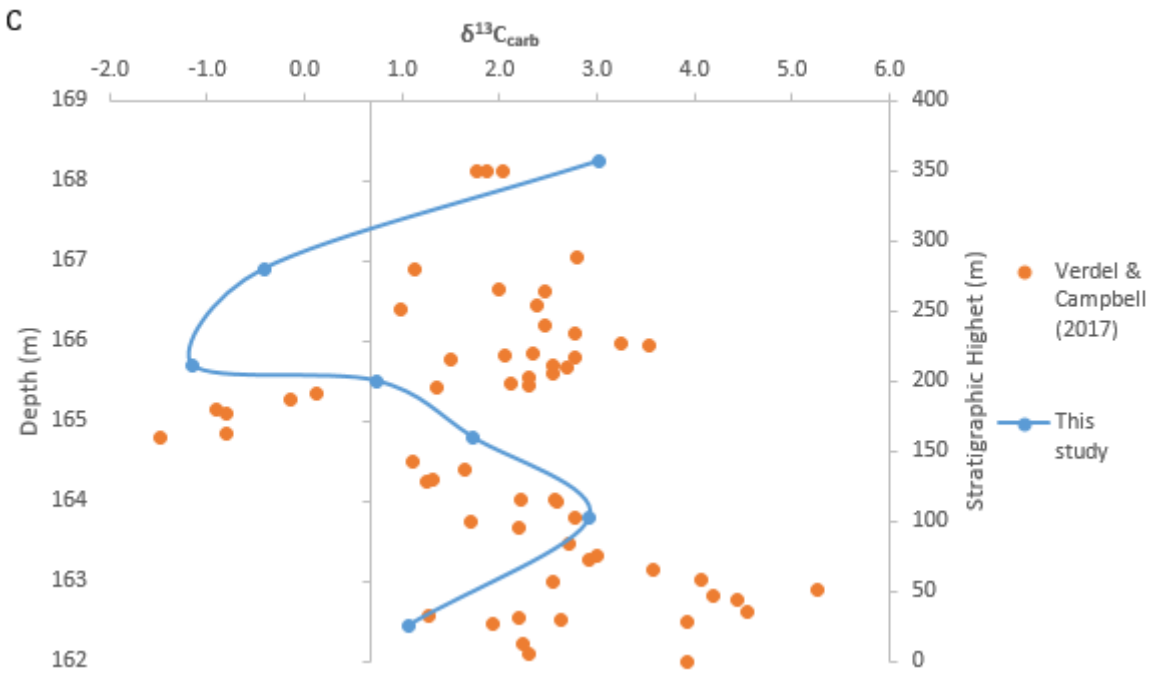

Figure 10: (A) comparison of $\delta^{13}C_{carb}$ data from BR05DD01 core from this study (blue circles and line) with data from Ringwood Member carbonates from NE part of the Amadeus Basin (orange circles = data from Verdel & Campbell (2017).

5.2. Correlation of Amadeus Basin $\delta^{13}C_{carb}$ Data with Global Marine C Isotope Records

The C isotope data obtained from this study can be correlated with global marine $\delta^{13}C_{carb}$ trend over the Neoproterozoic, which is shown in Figure 11 published data from Cox et al. (2016); Halverson et al. (2005, 2006), and local $\delta^{13}C_{carb}$ record from Verdel and Campbell (2017). As shown in Figure 11, the Bitter Spring Group has the same negative excursion as the other global data from the same time period, and similar agreements can be observed also for the other two studied sequences in the Amadeus Basin (Wallara Fm and Ringwood Member). As these also follow the global marine $\delta^{13}C_{carb}$ trend, where Wallara Formation had positive values and Ringwood Member $\delta^{13}C_{carb}$ values range from about -2 to 3 per mil, which overlaps with published data from Verdel and Campbell (2017).

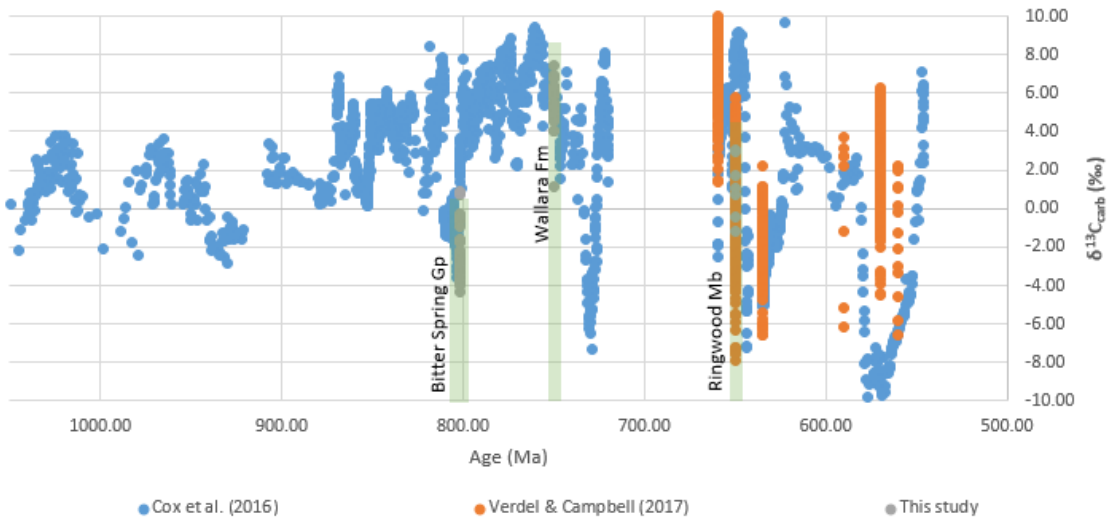

Figure 11: C isotope data from this study (grey circles) compared to local $\delta^{13}C_{carb}$ record from the Amadeus Bain (orange circles) by Verdel & Campbell (2017), and global $\delta^{13}C_{carb}$ record adapted from Cox et al. (2016). For the latter data comes from: Fike et al. 2006 (Buah Fm., Shuram Fm., and Khufai Fm., Oman), Halverson et al. 2005 (Karibib Fm., Hüttenberg Fm., Elandshoek Fm., and Maieberg Fm., Nambia), Swanson-Hysell et al. 2010 (Ombaatjie, Gruis, and Rasthof, Nambia), Halverson 2006 (Coppercap Fm., Mackenzies), Halverson et al. 2005 (Russøya Mb., Backlundtoppen Fm., Draken Fm., Svanbergfjellet Fm., and Grusdievbreen Fm., Svalbard), Halverson 2006 (Little Dal Group, NW Canada), Kuznetzov et al. 2006 (Karau Group, S. Urals), Macdonald et al. 2012 (Gibben Fm., Ogilvie Mountains), Knoll et al. 1995 (Derevnya, and Sukhaya Tunguska, Turukhansk), Knoll et al. 1995 (Linok, Turukhansk), and other unpublished data from Halverson.

5.3. Evaluation of Digenesis via Trace and Major Element Ratios

Post-depositional process such as meteoric diagenesis and/or clay contamination, and related in-situ Rb decay that can all change the $^{87}Sr/^{86}Sr$ signature in marine carbonates to more radiogenic values (Banner and Hanson, 1990; Nurgalieva et al., 2007) need to be carefully evaluated.

Numerous studies (Banner and Hanson, 1990; Halverson et al. 2007; Cox et al. 2016) stated that in order for marine carbonates to preserve original paleo-seawater Sr isotope signatures not altered by post-depositional process, these carbonates should have relatively low ratios of Rb/Sr and Mn/Sr (i.e. <0.1), and correspondently elevated Sr concentrations (e.g. >500 ppm). However, these

criteria cannot be always fulfilled and this also the case for most of the data obtained from the Amadeus Basin, where Mn/Sr and Rb/Sr ratios are generally high compared to the suggested values for well-preserved marine carbonates. These could be however also related to a proposed relative restriction of the Amadeus Basin, which thus received higher inputs of weathered and clay-derived cations (higher Rb/Sr ratios) and had perhaps also more reducing conditions (higher Mn/Sr) relative to coeval Neoproterozoic oceans.

Nevertheless, meotoric diagenesis effects were evaluated in this study via Mn/Sr ratio obtained from leached carbonates, and importantly data showed no obvious systematic relationship when plotted against $^{87}Sr/^{86}Sr$ values (see Figure 12), which thus more supports the above-mentioned basin restriction condition (more reducing paleo-depositional settings) rather than impact by meteoric diagenesis. As to clay contamination effects on $^{87}Sr/^{86}Sr$, these have been also monitored and evaluated via Al/Ca ratios, and data suggest some effects related to detrital contamination for carbonates from the Bitter Spring group and Ringwood Member from BR05DD01 core (Figure 12). However, data from Wallara-1 core show no obvious systematic relationship between Sr isotopes and Al/Ca ratios (Figure 12). Finally, Rb/Sr ratio showed strong positive correlation with $^{87}Sr/^{86}Sr$ values with all formation and in both cores studied (Figure 12), which in turn suggest that the Sr isotope data are likely also affected by the in-situ decay rubidium (^{87}Rb), which cause more production of radiogenic strontium (^{87}Sr) in the bulk carbonate rocks since their deposition. This study thus corrects all measured $^{87}Sr/^{86}Sr$ ratios for in-situ Rb decay using the following equation (Nurgalieva et al., 2007) see also the Method Section 3.5 for more details.

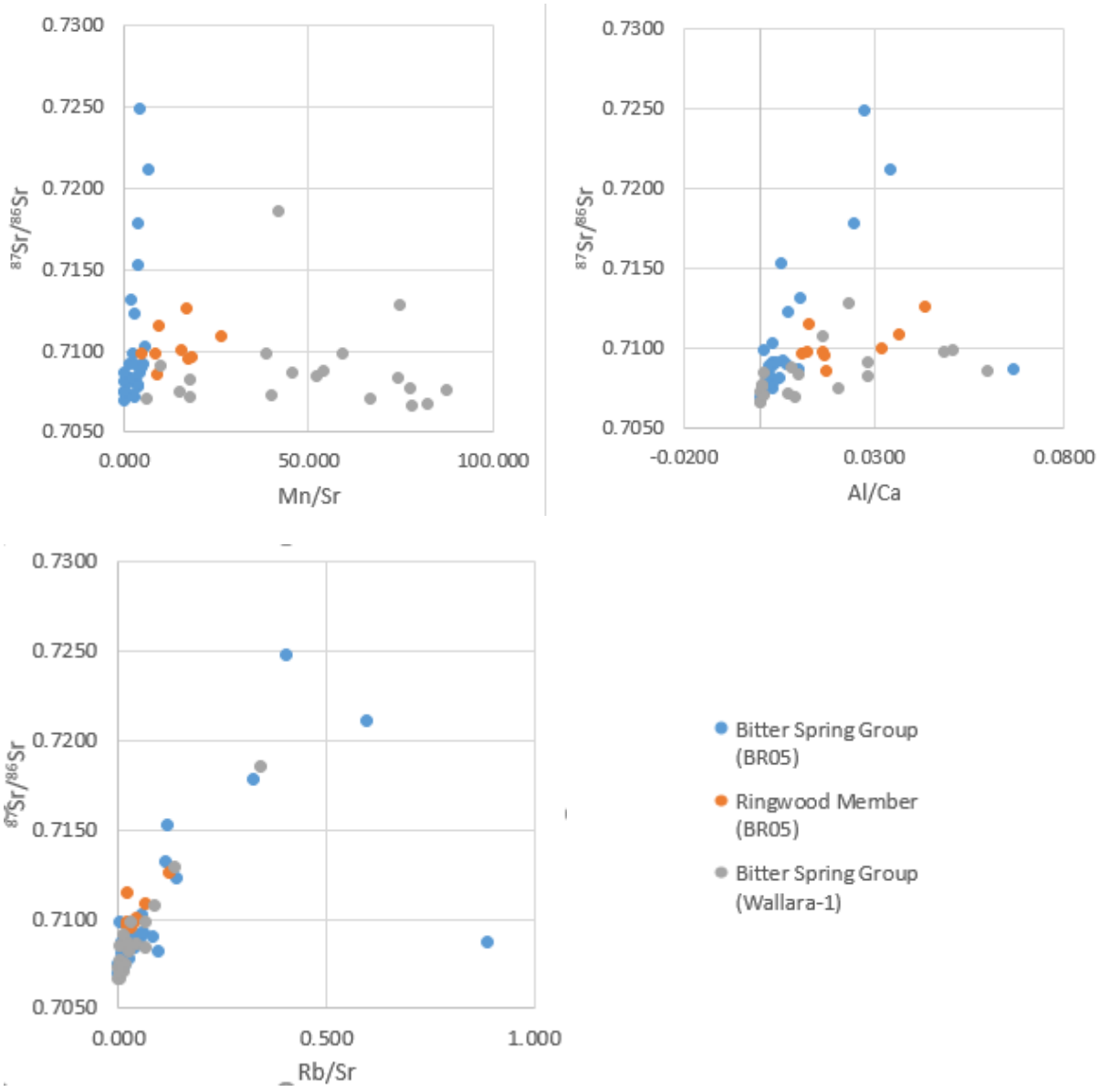

Figure 12: Measured elemental ratios (Mn/Sr, Al/Ca and Rb/Sr) plotted against $^{87}Sr/^{86}Sr$ for two formations (Bitter Spring Group and Ringwood Member) collected from two cores (BR05DD01 and Wallara-1).

5.4. Paleo-Redox Conditions Constrained from Ce/Ce* Anomalies

Paleo-depositional environments and past redox conditions (e.g., anoxic, oxic, euxinic, sub-oxic) can be constrained using redox-sensitive Rare Earth Element in marine carbonates and seawater such as cerium (Ce) (Zhang et al. 2015). Cerium (Ce) is characterized by having two oxidation states (+3) and (+4), which makes Ce deplete and oxidized in the presence of oxygen that leads to the removal of Ce from seawater onto the surfaces of Fe and Mn oxides. Modern

oceans typically have negative Ce/Ce* anomaly (i.e., less than 1) because of the modern oxic conditions, which thus results in the oxidation and depletion of Ce in seawater and marine carbonates. In the contrary, positive Ce/Ce* anomaly (more than 1) means Ce is not removed from ocean water due to possibly more anoxic condition (Wilde, Quinby-Hunt, & Erdtmann, 1996).

Following the method of Bau and Dulski (1996) the anomalies of Ce can be defined by cross-plotting Pr/Pr* versus Ce/Ce* and dividing to quadrants (see Figure 13). These can differentiate true negative Ce anomalies from La anomaly which has no implications for paleo-redox. Results of this study show that the Bitter Spring Group and Ringwood Member carbonate data generally have positive Ce anomalies (Figure 13) which indicate predominantly anoxic conditions during their deposition with limited O_2 availability or exchange between the surface-ocean and the atmosphere. However, a few values from Bitter Spring Group (from Wallara-1 core) exhibit true negative Ce anomalies, suggesting that the conditions were not entirely anoxic at that time and there were some locally more oxic conditions present.

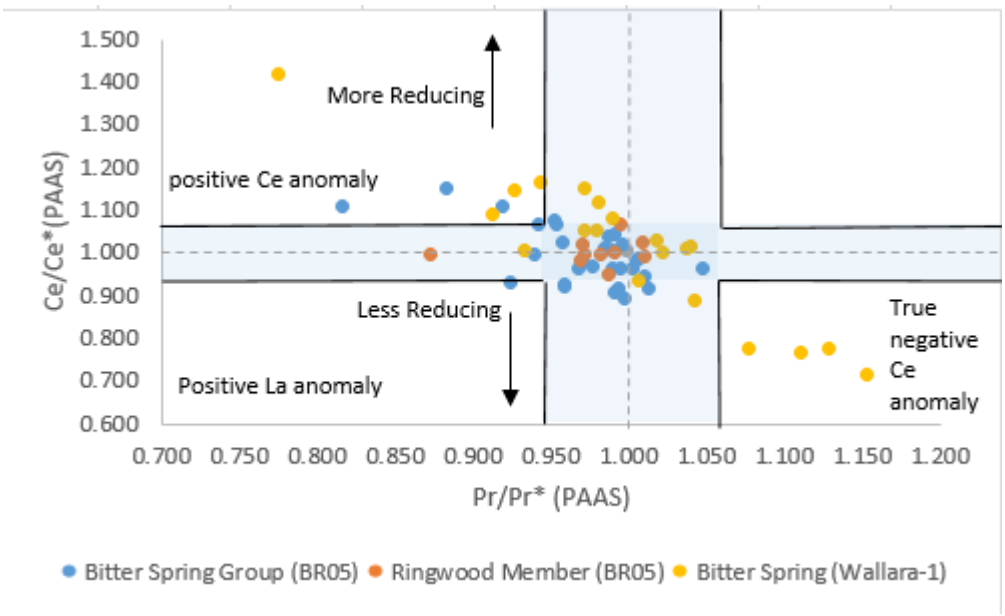

Figure 13: A cross plot of Ce/Ce*(PAAS) and Pr/Pr*(PAAS) data (normalized to Post-Archean Average Australian Shale, PAAS), where data are from two formations (Loves Creek Formation and Ringwood Member) and two wells (BR05DD01 and Wallara-1). Arrows shows less reducing (or more oxidizing) and more reducing.

Interestingly, theses samples with negative Ce anomaly comes from red beds within the Bitter Spring Group in Wallara-1 core, that shows strong indications of evaporative process and exposure (Klaebe, 2015) in presumably very shallow marine environments, which thus might explain the cause of these negative anomalies.

5.5. $^{87}Sr/^{86}Sr$ Data from the Amadeus Basin and Global Marine Sr Isotope Record

The $^{87}Sr/^{86}Sr$ data obtained by this study from the Amadeus Basin, are combined with $^{87}Sr/^{86}Sr$ data from the northeast part of the basin from previous studies (Love, 2017; Phelps, 2015) and plotted along with the global Neoproterozoic $^{87}Sr/^{86}Sr$ marine record (Figure 14). In general, these comparisons revealed that Sr isotope trend from the Amadeus Basin data evolves towards more radiogenic

values throughout the Neoproterozoic, relative to coeval global Sr isotope marine record. This in turn suggests that the intra-cratonic Amadeus Basin during the Neoproterozoic became more restricted from coeval open ocean, and this restriction was enhanced from Tonian towards Cryogenian/Ediacaran as suggested by data in Figure 14. However, some Sr isotope data from Bitter Spring Group overlaps or approach the global seawater Sr isotope curve, suggesting that during these times (Tonian, around 800 Ma ago) at least parts of the basin were likely at some level connected with the global ocean although conditions during deposition of Bitter Spring Formation indicate evaporitic settings (perhaps pointing to "evaporitic seaway" conditions during this time). Overall, the global seawater $^{87}Sr/^{86}Sr$ record has limited use in the Amadeus Basin from stratigraphic prospective, which thus suggests the need for constructing a local Sr isotope curve specific for this intra-cratonic depositional system that could be used then for future chemostratigraphic studies in the Amadeus Basin and its carbonate-rich sequences.

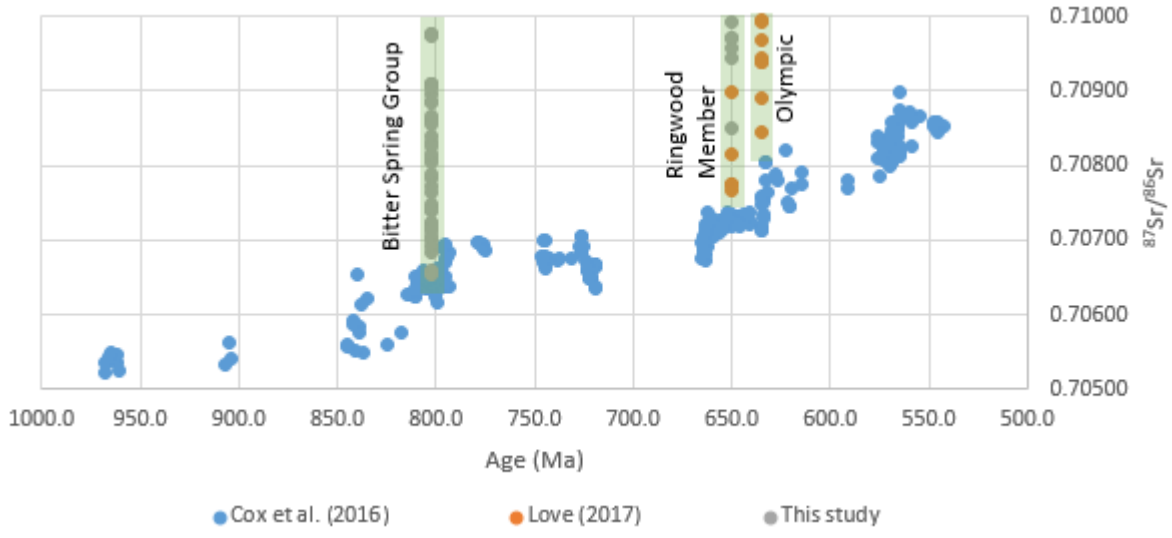

Figure 14: Global $^{87}Sr/^{86}Sr$ Neoproterozoic marine record (blue circles) adapted from Cox et al. (2016) compared to data from the Amadeus Basin (our data, plus data from Love, 2017).

6. CONCLUSIONS

This study investigated $^{87}Sr/^{86}Sr$ and $\delta^{13}C$ isotope trends from Neoproterozoic carbonates from the Amadeus Basin (from two cores BR05DD01 and Wallara-1) and compared them to published local records (i.e., from NE part of the Amadeus Basin) and also to global marine C and Sr isotope trends. Overall, our $\delta^{13}C$ trends from above drill cores can be correlated well with both local and global Neoproterozoic C isotope records, however $^{87}Sr/^{86}Sr$ data from this study appeared to be more radiogenic than global seawater Sr isotope record. One of the reasons for this discrepancy is likely related to in-situ Rb decay in the studied bulk samples (with elevated Rb/Sr ratios), which would lead over time to more radiogenic $^{87}Sr/^{86}Sr$ of bulk carbonates. However, after applying correction for in-situ Rb decay to our measured $^{87}Sr/^{86}Sr$ data, the latter are still systematically more radiogenic compared to expected global marine Sr isotope record. This in turn suggest relative restriction of the Amadeus Basin during the Neoproterozoic, and data indicate that such restriction became more enhanced during the Cryogenian/Ediacaran, and was likely less pronounced during Tonian. Furthermore, the Ringwood Member from Aralka Formation yielded $\delta^{13}C_{carb}$ values from BR05DD01 core that can be correlated with local C isotope data of the same sequence (Ringwood Mb) from the northeast parts of the Amadeus Basin, which thus supports the proposition that the formation between 500-200 m in BR05DD01 core is indeed the Aralka Formation (with Ringwood Mb) and not Pertatataka Formation.

In summary, the paleo-depositional environment and past redox conditions during carbonate deposition of the Bitter Spring Group and Ringwood Member (based on records from two cores BR05DD01 and Wallara-1) was constrained using $^{87}Sr/^{86}Sr$

and Ce/Ce* proxies, together with major and trace elements concentrations. Results from the above redox-sensitive traces and $^{87}Sr/^{86}Sr$ showed that during the deposition of the Bitter Spring Group and Ringwood Member the paleo-depositional environment in these parts of the Amadeus Basin was mostly anoxic and predominantly restricted (with respect to the coeval open ocean). Overall, this study showed that correlated carbonates sequences from different cores in the Amadeus Basin exhibit basin-wide C and Sr patterns (with similarities to global isotope trends, especially for C isotopes), which can thus be used for future detail chemostratigraphic studies in the Amadeus Basin.

7. ACKNOWLEDGMENTS

I would like acknowledge Santos Ltd. and University of Adelaide for funding this project. I also would like to thank everyone who helped me academically or personally throughout this year. Special thanks to my supervisors Juraj Farkas and Grant Cox. Many thanks to everyone who helped me collecting my samples from NTGS. Distinct thanks to David Bruce for his tireless assistance in the clean lab, and Phil Plummer for initial discussion regarding this project and relevant research questions. Also thanks to lab assistance, Tony Hall, Mark Rollog, and Sarah Gilbert from Adelaide Microscopy. I also acknowledge Prof. Galen Halverson and Dr. Thi Hao Bui at McGill Uni for C and O isotope analysis of carbonates from BR05DD01 core. Finally, assistance and advice of Drs. Chris Edgoose, Dorothy Close and Verity Normington from NTGS, regarding a revised Neoproterozoic stratigraphy of the Amadeus Basin and selection of suitable samples, are also greatly acknowledged.

8. REFERENCES

AMBROSE, G., DANSTER, J., MUNSON, T. and EDGOOSE, C. (2010). Well completion reports for NTGS stratigraphic drillholes LA05DD01 and BR05DD01, southeastern Amadeus Basin, *Northern Territory Geological Survey, Record* 2010-015.

BANNER, J., & HANSON, G. (1990). Calculation of simultaneous isotopic and trace element variations during water-rock interaction with applications to carbonate diagenesis. *Geochimica et Cosmochimica Acta, 54*(11), 3123-3137.

BAU, M., & DULSKI, P. (1996). Distribution of yttrium and rare-earth elements in the Penge and Kuruman ironformations, Transvaal Supergroup, South Africa. *Precambrian Research, 79*(1), 37-55. doi:https://doi.org/10.1016/0301-9268(95)00087-9

CALVER, C. (1998). Isotope stratigraphy of the Neoproterozoic Togari Group, Tasmania. Australian *Journal of Earth Sciences, 45*(6), 865-874.

CALVER, C. (2000). Isotope stratigraphy of the Ediacarian (Neoproterozoic III) of the Adelaide Rift Complex, Australia, and the overprint of water column stratification. *Precambrian Research, 100*(1), 121-150.

COX, G., HALVERSON, G., STEVENSON, R., VOKATY, M., POIRIER, A., KUNZMANN, M., & MACDONALD, F. (2016). Continental flood basalt weathering as a trigger for Neoproterozoic Snowball Earth. . *Earthand Planetary Science Letters,* (446), 89-99. doi: 10.1016/j.epsl.2016.04.016

FIKE, D. A., GROTZINGER, J. P., PRATT, L. M., SUMMONS, R. E. (2006). Oxidation of the Edi-acaran Ocean. *Nature44*, 744–747.

HALVERSON, G. P., HOFFMAN, P. F., SCHRAG, D. P., MALOOF, A. C., RICE, A. H. (2005). Toward a Neoproterozoic composite carbon-isotope record. *Geol. Soc. Am., 117*, 1181–1207.

HALVERSON, G. (2006). A Neoproterozoic chronology. In: Neoproterozoic Geobiology and Paleobiology, 231–271.

HALVERSON, G. P., DUDAS, F. O., MALOOF, A. C., BOWRING, S. A. (2007). Evolution of the $^{87}Sr/^{86}Sr$ composition of Neoproterozoic seawater. *Palaeogeogr. Palaeoclimatol. Palaeoecol, 256,* 103-129.

HALVERSON, G.P., WADE, B.P., HURTGEN, M.T., & BAROVICH, K.M. (2010). Neoproterozoic chemostratigraphy, *Precambrian Research*, 182, 337–350, doi:10.1016/j.precamres.2010.04.007.

KENNEDY, M. J. (1996). Stratigraphy, sedimentology, and isotopic geochemistry of Australian Neoproterozoic postglacial cap dolostones: deglaciation, d13C excursions, and carbonate precipitation. *Journal of sedimentary Research, 66(6*). doi: http://archives.datapages.com/data/sepm/journals/v66-67/data/066/066006/1050.htm?doi=10.1306%2FD42684A5-2B26-11D7-8648000102C1865D

KENNEDY, M.J., CHRISTIE-BLICK, N., & PRAVE, A.R. (2001). Carbon isotopic composition of Neoproterozoic glacial carbonates as a test of paleoceanographic models for snowball Earth phenomena: Geology, 29, 1135–1138, doi:10.1130/0091-7613(2001)029<1135:CICONG>2.0.CO;2.

KLAEBE, R. (2015).*The Paleoenvironmental Context Of Neoproterozoic Carbon-Isotope Excursions.* (PhD), The University of Adelaide.

KUZNETSOV, A. B., SEMIKHATOV, M. A., MASLOV, A. V., GOROKHOV, I. M., PRASOLOV, E. M., KRU-PENIN, M. T., KISLOVA, I. V. (2006). New data on Sr-and C-isotopic chemostratig-raphy of the Upper Riphean type section (Southern Urals). *Stratigr. Geol. Cor-rel., 14*, 602–628.

KUZNESTSOV, A.B., SEMIKHATOV M.A. and GOROKHOV I.M. (2018) Strontium Isotope Stratigraphy: Principles and State of the Art. In: Stratigraphy and Geological Correlation, 2018, Vol. 26, No. 4, p. 367-386. Pletades Publishing. ISSN 0869-5938.

KNOLL, A. H., KAUFMAN, A. J., SEMIKHATOV, M. A. (1995). The carbon-isotopic composition of Proterozoic carbonates; Riphean successions from northwestern Siberia (An-abar Massif, Turukhansk Uplift). *Am. J. Sci., 295*, 823–850.

LIU, C., WANG, Z., & RAUB, T. D. (2013). Geochemical constraints on the origin of Marinoan cap dolostones from Nuccaleena Formation, South Australia. *Chemical Geology, 351*, 95-104. doi: 10.1016/j.chemgeo.2013.05.012

LIU, C., WANG, Z., RAUB, T. D., MACDONALD, F. A., & EVANS, D. A. D. (2014). Neoproterozoic cap-dolostone deposition in stratified glacial meltwater plume. *Earth and Planetary Science Letters, 404*, 22-32. doi: https://doi.org/10.1016/j.epsl.2014.06.039

LOVE, A. (2017). *Strontium Isotope Constraints on the Neoproterozoic Stratigraphy of the Amadeus Basin*. (BSc (Honours)), The University of Adelaide.

MACDONALD, F.A., JONES, D.S., AND SCHRAG, D.P. (2009), Stratigraphic and tectonic implications of a newly discovered glacial diamictite–cap carbonate couplet in south western Mongolia, *Geology*, 37(2), 123–126, doi:10.1130/G24797A.1

MACDONALD, F. M., HALVERSON, G. P., STRAUSS, J. V., SMITH, E. F., COX, C. M., SPERLING, E., ROOTS, C. F., SCHRAG, D. P. (2012). Early Neoproterozoic basin formation in the Yukon: implications for the make-up and break-up of Rodinia. *Geosci. Can., 39*, 77–97.

MADIGAN, C.T. (1932). The geology of the Western MacDonnell Ranges, Central Australia. *Quarterly Journal of the Geological Sciences of London 88*, 672-711.

MCARTHUR J.M., HOWARD R.J. and SHIELDS G.A. (2012) Strontium Isotope Stratigraphy, In: The Geological Time Scale 2012. DOI: 10.1016/B978-0-444-59425-9.00007-X. Eds: F.M. Gradstein and J.G. Ogg; Elsevier.

MCKIRDY, D., BURGESS, J., LEMON, N., YU, X., COOPER, A., GOSTIN, V., . . . BOTH, R. (2001). A chemostratigraphic overview of the late Cryogenian interglacial sequence in the Adelaide Fold-ThrustBelt, South Australia. *Precambrian Research, 106*(1), 149-186. doi: https://doi.org/10.1016/S0301-9268(00)00130-3

NEUMANN, W., AND HUSTER, E. (1974). The half-life of ^{87}Rb measured as difference between the isotopes ^{87}Rb and ^{85}Rb, Z. *Physik*, 270, 121, doi:10.1007/BF01677443.

NORMINGTON, V. Revised stratigraphy of drillholes CPDD001, CPDD002 and CPDD003, Pipeline Prospect, northeast Amadeus Basin. *Northern Territory Geological Survey*.

NORMINGTON, V. and EDGOOSE, C. (2018). Neoproterozoic stratigraphic revisions to key drillholes in the Amadeus Basin – implication for the Basin paleogeography and petroleum and mineral potential. *Annual Geoscience Exploration Seminar.* 108-112.

NURGALIEVA, N. G., PONOMARCHUK, V. A., & NURGALIEV, D. K. (2007). Strontium isotope stratigraphy: Possible applications for age estimation and global correlation of Late Permian carbonates of the Pechishchi type section, Volga River. Russian Journal of Earth Sciences., 9(Russian Journal of Earth Sciences.). doi:10.2205/2007ES000221

OEHLER, D.Z., OEHLER, J.H., STEWART, A.J. (1979). Algal fossils from the late precambrian, hypersaline lagoon. *Science 205*, 388–390.

PHELPS (2015). Strontium isotope and trace element constraints on Neoproterozoic carbonates in the Amadeus Basin, central Australia. (BSc (Honours)), The University of Queensland.

PLUMMER, P. (2018). Seismic shift in regional Neoproterozoic correlation, *Annual Geoscience Exploration Seminar.* 96-107..

PREISS, W.V., WALTER, M.R., COATS, R.P., & WELLS, AT. (1978). Lithological correlations of Adelaidean glaciogenic rocks in parts of the Amadeus, Ngalia and Georgina basins. *Bureau of Mineral Resources, Journal of Australian Geology and Geophysics* 3, 43-53.

PRICHARD, C.E. & QUINLAN, T. (1960). The geology of the southern part of the Hermannsberg 4-mile sheet. *Bureau of Mineral Resources, Geology and Geophysics, Record 1960/104*

RAMKUMAR, M., & AINSAAR, LEHO, CONTRIBUTOR. (2015). *Chemostratigraphy: Concepts, techniques, and applications / edited by Mu Ramkumar ; contributors Leho Ainsaar [and forty eight others]*.

SCHMID, S., SCHAUBS, P., AUSTIN, J., FOSS, C., GRAY, D.J., LAUKAMP, C., KEMPTON, R., BOURDET, J., TERFRY, C., LEGRAS, M., COBRA – Amadeus Basin Assessment of resources potential. Northern Territory Geological Survey, DIP016, 478p.

SCHMID, S. (2017). Neoproterozoic evaporites and their role in carbon isotope chemostratigraphy (Amadeus Basin, Australia). *Precambrian Research, 290*, 16-31

SOUTHGATE, P.N. (1986). Depositional environment and mechanism of preservation of microfossils, upper Proterozoic Bitter Springs Formation, Australia. *Geology 14*, 683–686.

SOUTHGATE, P.N. (1989). Relationship between cyclicity and stromatolite form in the Late Proterozoic Bitter Springs Formation, Australia. *Sedimentology 36*, 323–339.

SWANSON-HYSELL, N.L., ROSE, C.V., CALMET, C.C., HALVERSON, G.P., HURTGEN, M.T., AND MALOOF, A.C. (2010), Cryogenian glaciation and the onset of carbon-isotope decoupling, *Science*, 328, 608–611, doi:10.1126/ science.1184508

TAYLOR, S.R., MCCLENNAN, S.M. (1985). The Continental Crust: Its Composition and Evolution, p.312.

Tostevin, R., Shields, G. A., Tarbuck, G. M., He, T., Clarkson, M. O., & Wood, R. A. (2016). Effective use of cerium anomalies as a redox proxy in carbonate-dominated marine settings. *Chemical Geology*, 438, 146-162.

VERDEL, C., & CAMPBELL, M. (2017). Neoproterozoic carbon isotope stratigraphy of the Amadeus Basin, central Australia. *The Geological Society of America Bulletin, 129*(9-10), 1280-1299

WALTER, M.R. (1972). Stromatolites and the biostratigraphy of the Australian Precambrian and Cambrian. Spec. Pap. *Palaeontol*. 11, 139.

WELLS, A.T., RANFORD, L.C., STEWART, A.J., COOK, P.J, SHAW, R.D. (1967). Geology of the North-Eastern Part of the Amadeus Basin, Northern Territory. *Department National Devolpment Bureau of Mineral Resources Geology and Geophysics 113*, 26-27.

WILDE, P., QUINBY-HUNT, M. S., & ERDTMANN, B.-D. (1996). The whole-rock cerium anomaly: a potential indicator of eustatic sea-level changes in shales of the anoxic facies. *Sedimentary Geology, 101*(1-2), 43-53.

UNPUBLISHED.

WALTER, M., VEEVERS, J., CALVER, C., GORJAN, P., & HILL, A. (2000). Dating the 840–544 Ma Neoproterozoic interval by isotopes of strontium, carbon, and sulfur in seawater, and some interpretative models. *Precambrian Research, 100(*1), 371-433.

9. APPENDIX A: SAMPLES IDENTITIES (IDS)

Core Name	latitude	Longitude	Sample ID	Depth (m)	Stratigraphy
BR05DD01	-24.4556878	130.3825099	BR1	1193.3	Loves Creek Fm.
BR05DD01	-24.4556878	130.3825099	BR2	1191	Loves Creek Fm.
BR05DD01	-24.4556878	130.3825099	BR3	1186.1	Loves Creek Fm.
BR05DD01	-24.4556878	130.3825099	BR4	1184.55	Loves Creek Fm.
BR05DD01	-24.4556878	130.3825099	BR5	1179.4	Loves Creek Fm.
BR05DD01	-24.4556878	130.3825099	BR6	1178.8	Loves Creek Fm.
BR05DD01	-24.4556878	130.3825099	BR7	1176.4	Loves Creek Fm.
BR05DD01	-24.4556878	130.3825099	BR8	1174.1	Loves Creek Fm.
BR05DD01	-24.4556878	130.3825099	BR9	1170.3	Loves Creek Fm.
BR05DD01	-24.4556878	130.3825099	BR11	1163.73	Loves Creek Fm.
BR05DD01	-24.4556878	130.3825099	BR13	1157.67	Loves Creek Fm.
BR05DD01	-24.4556878	130.3825099	BR15	1151.4	Loves Creek Fm.
BR05DD01	-24.4556878	130.3825099	BR16	1149	Loves Creek Fm.

BR05DD01	-24.4556878	130.3825099	BR17	1143.3	Loves Creek Fm.
BR05DD01	-24.4556878	130.3825099	BR19	1131.8	Loves Creek Fm.
BR05DD01	-24.4556878	130.3825099	BR21	1123.9	Loves Creek Fm.
BR05DD01	-24.4556878	130.3825099	BR22	1122.7	Loves Creek Fm.
BR05DD01	-24.4556878	130.3825099	BR24	1117.6	Loves Creek Fm.
BR05DD01	-24.4556878	130.3825099	BR25	1112	Loves Creek Fm.
BR05DD01	-24.4556878	130.3825099	BR26	1108.83	Loves Creek Fm.
BR05DD01	-24.4556878	130.3825099	BR27	1106.62	Loves Creek Fm.
BR05DD01	-24.4556878	130.3825099	BR28	1102.9	Loves Creek Fm.
BR05DD01	-24.4556878	130.3825099	BR29	1099.2	Loves Creek Fm.
BR05DD01	-24.4556878	130.3825099	BR32	1091.21	Loves Creek Fm.
BR05DD01	-24.4556878	130.3825099	BR35	1087.2	Loves Creek Fm.
BR05DD01	-24.4556878	130.3825099	BR37	1082.6	Loves Creek Fm.
BR05DD01	-24.4556878	130.3825099	BR39	1077.1	Loves Creek Fm.
BR05DD01	-24.4556878	130.3825099	BR40	1074.8	Loves Creek Fm.
BR05DD01	-24.4556878	130.3825099	BR41	1072.55	Loves Creek Fm.
BR05DD01	-24.4556878	130.3825099	BR42	1070.04	Loves Creek Fm.
BR05DD01	-24.4556878	130.3825099	BR189	192.5	Ringwood Member
BR05DD01	-24.4556878	130.3825099	BR191	189.6	Ringwood Member
BR05DD01	-24.4556878	130.3825099	BR193	187.95	Ringwood Member
BR05DD01	-24.4556878	130.3825099	BR205	173.6	Ringwood Member
BR05DD01	-24.4556878	130.3825099	BR213	164.8	Ringwood Member
BR05DD01	-24.4556878	130.3825099	BR216	162.45	Ringwood Member
BR05DD01	-24.4556878	130.3825099	BR218	160.15	Ringwood Member

BR05DD01	-24.4556878	130.3825099	BR219	159	Ringwood Member
BR05DD01	-24.4556878	130.3825099	BR223	155.7	Ringwood Member
Wallara-1	24° 36' 54.99"	132° 20' 23.01"	W1	1957.8	Loves Creek Fm.
Wallara-1	24° 36' 54.99"	132° 20' 23.01"	W2	1953.52	Loves Creek Fm.
Wallara-1	24° 36' 54.99"	132° 20' 23.01"	W3	1952.3	Loves Creek Fm.
Wallara-1	24° 36' 54.99"	132° 20' 23.01"	W4	1951.65	Loves Creek Fm.
Wallara-1	24° 36' 54.99"	132° 20' 23.01"	W5	1951.3	Loves Creek Fm.
Wallara-1	24° 36' 54.99"	132° 20' 23.01"	W6	1950.6	Loves Creek Fm.
Wallara-1	24° 36' 54.99"	132° 20' 23.01"	W7	1949.58	Loves Creek Fm.
Wallara-1	24° 36' 54.99"	132° 20' 23.01"	W8	1948.6	Loves Creek Fm.
Wallara-1	24° 36' 54.99"	132° 20' 23.01"	W9	1948.26	Loves Creek Fm.
Wallara-1	24° 36' 54.99"	132° 20' 23.01"	W10	1946.75	Loves Creek Fm.
Wallara-1	24° 36' 54.99"	132° 20' 23.01"	W11	1945	Loves Creek Fm.
Wallara-1	24° 36' 54.99"	132° 20' 23.01"	W12	1944.4	Loves Creek Fm.
Wallara-1	24° 36' 54.99"	132° 20' 23.01"	W13	1942.96	Loves Creek Fm.
Wallara-1	24° 36' 54.99"	132° 20' 23.01"	W14	1941.25	Loves Creek Fm.
Wallara-1	24° 36' 54.99"	132° 20' 23.01"	W15	1940.5	Loves Creek Fm.
Wallara-1	24° 36' 54.99"	132° 20' 23.01"	W16	1938.47	Loves Creek Fm.
Wallara-1	24° 36' 54.99"	132° 20' 23.01"	W17	1936.65	Loves Creek Fm.
Wallara-1	24° 36' 54.99"	132° 20' 23.01"	W18	1933.75	Loves Creek Fm.
Wallara-1	24° 36' 54.99"	132° 20' 23.01"	W19	1932.8	Loves Creek Fm.
Wallara-1	24° 36' 54.99"	132° 20' 23.01"	W20	1930.4	Loves Creek Fm.

10. APPENDIX B: EXTENDED METHODS

$^{87}Sr/^{86}Sr$ Isotope Extended Method

Standard column procedure was followed in preparation of dolomite samples, where standard safety and health were followed carefully (see the instructions below for the whole process). The maximum number of samples that were in one batch was 40, which then were dried and made ready for filament loading and TIMS analysis.

Sr Micro Bio-Spin column procedure
Remove columns from 1M HNO3 storage container using blue PP forceps.
Rinse 3 times with DI water and place into racks.
Load 200uL Sr Resin SPS (1/3 narrow column section) using 1mL pipette.
Avoid bubbles in the resin bed.
Wash resin and column with 3mL 8M HNO3 sd
Wash resin and column with 3mL DI H2O
Wash resin and column with 3mL 8M HNO3 sd
Wash resin and column with 3mL DI H2O
Equilibrate resin with 3mL 8M HNO3 sd
Load sample in 1mL 8M HNO3 sd
5 x wash with 1mL 8M HNO3
Collect Sr with 6x 0.05M HNO3 sd
Add 1 drop 0.1M H3PO4 to Sr vial. (Also remember to spike any blanks)
Dry on hot plate at ≤ 140C
Add squirt (0.5mL) of 15M HNO3 + 0.25mL H2O2 to oxidize any organics. Cap vials and heat at 110C for at least 5 hours.
Dry on hot plate at ≤ 140C
Remove columns to waste.
Rinse racks etc with DI water, dry then return to storage container(s).

TIMS Analysis

All the filaments were welded and then degassed for one day before loading the samples. The loading procedure is described below.

1- Centre Re Filament in non-zone-refined Re ribbon
2- Load 1uL 1M H_3PO_4 and evaporate at 0.5A.
3- Load 0.5uL Bircks solution and evaporate.
4- Load Sample in 1uL Bircks solution and dry at 0.5A.
5- Gradually increase to 1A.
6- Increase to 1.8A, after 1 minute.
7- Heat till the sample turn red.
8- The sample is ready to be loaded in TIMS.

11. APPENDIX C: ISOTPES DATA

Carbon and Oxygen isotopes

Sample Name	Core Name	Depth (m)	Formation	sub-Class	$d^{13}C\_vpdb$	$d^{18}O\_vpdb$
BR-1	BR05DD01	1193.3	Bitter Spring Gr	Loves Creek Fm	-3.714	-6.361
BR-2	BR05DD01	1191	Bitter Spring Gr	Loves Creek Fm	-3.427	-6.114
BR-3	BR05DD01	1186.1	Bitter Spring Gr	Loves Creek Fm	-4.312	-6.536
BR-4	BR05DD01	1184.55	Bitter Spring Gr	Loves Creek Fm	-3.537	-6.482
BR-5	BR05DD01	1179.4	Bitter Spring Gr	Loves Creek Fm	-3.131	-6.162
BR-6	BR05DD01	1178.8	Bitter Spring Gr	Loves Creek Fm	-3.040	-6.323
BR-7	BR05DD01	1176.4	Bitter Spring Gr	Loves Creek Fm	-3.799	-8.317
BR-8	BR05DD01	1174.1	Bitter Spring Gr	Loves Creek Fm	-3.530	-6.174
BR-9	BR05DD01	1170.3	Bitter Spring Gr	Loves Creek Fm	-2.460	-5.939
BR-10	BR05DD01	1165.7	Bitter Spring Gr	Loves Creek Fm	-3.526	-6.232
BR-11	BR05DD01	1163.73	Bitter Spring Gr	Loves Creek Fm	-3.505	-5.915
BR-12	BR05DD01	1159.4	Bitter Spring Gr	Loves Creek Fm	-3.429	-6.021
BR-13	BR05DD01	1157.67	Bitter Spring Gr	Loves Creek Fm	-3.482	-6.080
BR-14	BR05DD01	1154.5	Bitter Spring Gr	Loves Creek Fm	-3.378	-6.068
BR-15	BR05DD01	1151.4	Bitter Spring Gr	Loves Creek Fm	-0.693	-8.382
BR-16	BR05DD01	1149	Bitter Spring Gr	Loves Creek Fm	-2.747	-5.844
BR-17	BR05DD01	1143.3	Bitter Spring Gr	Loves Creek Fm	-3.179	-6.241
BR-18	BR05DD01	1137.7	Bitter Spring Gr	Loves Creek Fm	-3.986	-7.919
BR-19	BR05DD01	1131.8	Bitter Spring Gr	Loves Creek Fm	-2.978	-5.534
BR-20	BR05DD01	1128	Bitter Spring Gr	Loves Creek Fm	-3.735	-7.063
BR-21	BR05DD01	1123.9	Bitter Spring Gr	Loves Creek Fm	-2.689	-4.060
BR-22	BR05DD01	1122.7	Bitter Spring Gr	Loves Creek Fm	-2.752	-5.429

BR-23	BR05DD01	1119.5	Bitter Spring Gr	Loves Creek Fm	-3.700	-7.197
BR-24	BR05DD01	1117.6	Bitter Spring Gr	Loves Creek Fm	-2.641	-5.961
BR-25	BR05DD01	1112	Bitter Spring Gr	Loves Creek Fm	-2.808	-5.618
BR-26	BR05DD01	1108.83	Bitter Spring Gr	Loves Creek Fm	-1.682	-4.537
BR-27	BR05DD01	1106.62	Bitter Spring Gr	Loves Creek Fm	-2.513	-5.442
BR-28	BR05DD01	1102.9	Bitter Spring Gr	Loves Creek Fm	-2.662	-8.023
BR-29	BR05DD01	1099.2	Bitter Spring Gr	Loves Creek Fm	-2.337	-5.342
BR-30	BR05DD01	1097.3	Bitter Spring Gr	Loves Creek Fm	-2.801	-7.049
BR-32	BR05DD01	1091.21	Bitter Spring Gr	Loves Creek Fm	-2.928	-6.084
BR-33	BR05DD01	1090.5	Bitter Spring Gr	Loves Creek Fm	-0.234	-4.005
BR-34	BR05DD01	1087.8	Bitter Spring Gr	Loves Creek Fm	-1.756	-7.083
BR-35	BR05DD01	1087.2	Bitter Spring Gr	Loves Creek Fm	0.724	-4.354
BR-36	BR05DD01	1085.99	Bitter Spring Gr	Loves Creek Fm	-1.671	-6.896
BR-37	BR05DD01	1082.6	Bitter Spring Gr	Loves Creek Fm	-1.578	-5.521
BR-38	BR05DD01	1079.1	Bitter Spring Gr	Loves Creek Fm	-0.495	-5.381
BR-39	BR05DD01	1077.1	Bitter Spring Gr	Loves Creek Fm	0.884	-6.493
BR-40	BR05DD01	1074.8	Bitter Spring Gr	Loves Creek Fm	-2.138	-7.504
BR-41	BR05DD01	1072.55	Bitter Spring Gr	Loves Creek Fm	-0.895	-5.143
BR-42	BR05DD01	1070.04	Bitter Spring Gr	Loves Creek Fm	-0.469	-5.340
BR-131	BR05DD01	676.4	Wallara Fm		5.176	-1.509
BR-132	BR05DD01	673	Wallara Fm		4.013	-3.480
BR-133	BR05DD01	671.1	Wallara Fm		5.220	-0.645
BR-134	BR05DD01	665.8	Wallara Fm		4.996	-2.671
BR-135	BR05DD01	663.8	Wallara Fm		6.046	-1.398

BR-136	BR05DD01	661.4	Wallara Fm		5.050	-0.933
BR-137	BR05DD01	659.1	Wallara Fm		5.207	-2.966
BR-138	BR05DD01	657.15	Wallara Fm		6.349	-1.823
BR-139	BR05DD01	655.1	Wallara Fm		5.542	-2.151
BR-140	BR05DD01	654.3	Wallara Fm		4.833	-2.224
BR-141	BR05DD01	651.8	Wallara Fm		5.850	-1.897
BR-142	BR05DD01	648.4	Wallara Fm		5.860	-0.818
BR-143	BR05DD01	645.1	Wallara Fm		4.707	-1.384
BR-144	BR05DD01	637.7	Wallara Fm		6.975	-1.641
BR-145	BR05DD01	635.5	Wallara Fm		6.791	-1.591
BR-146	BR05DD01	630.1	Wallara Fm		1.112	-4.808
BR-147	BR05DD01	624.6	Wallara Fm		4.505	-3.152
BR-148	BR05DD01	623.6	Wallara Fm		5.399	-2.293
BR-149	BR05DD01	610.6	Wallara Fm		6.359	-2.753
BR-150	BR05DD01	607.75	Wallara Fm		4.002	-5.081
BR-151	BR05DD01	602.4	Wallara Fm		5.481	-2.971
BR-152	BR05DD01	595.35	Wallara Fm		7.431	-7.559
BR-153	BR05DD01	587.1	Wallara Fm		6.080	-5.050
BR-154	BR05DD01	572.4	Wallara Fm		6.733	-4.476
BR-155	BR05DD01	564.4	Wallara Fm		5.307	-3.168
BR-156	BR05DD01	553.9	Wallara Fm		6.308	-5.699
BR-157	BR05DD01	553.2	Wallara Fm		4.928	-5.868
BR-209	BR05DD01	168.25	Aralka/Ringwood		3.026	-3.054
BR-210	BR05DD01	166.9	Aralka/Ringwood		-0.419	-1.261

BR-211	BR05DD01	165.7	Aralka/Ringwood		-1.152	-1.415
BR-212	BR05DD01	165.5	Aralka/Ringwood		0.737	-1.934
BR-213	BR05DD01	164.8	Aralka/Ringwood		1.718	-4.046
BR-214	BR05DD01	163.8	Aralka/Ringwood		2.919	-1.855
BR-216	BR05DD01	162.45	Aralka/Ringwood		1.067	-2.026

Strontium Isotope Data

Sample ID	Depth (m)	Stratigraphy	Sr_ppm	87/86 Sr	2Se	87Sr/86Sr (Rb-decay corr)
BR1	1193.3	Loves Creek Fm.	29.619	0.7284	0.000007	0.7177
BR2	1191	Loves Creek Fm.	46.068	0.7112	0.000013	0.7091
BR3	1186.1	Loves Creek Fm.	18.963	0.7168	0.000291	0.7122
BR4	1184.55	Loves Creek Fm.	30.536	0.7404	0.000008	0.7211
BR5	1179.4	Loves Creek Fm.	52.022	0.7102	0.000005	0.7091
BR6	1178.8	Loves Creek Fm.	39.337	0.7106	0.000028	0.7089
BR7	1176.4	Loves Creek Fm.	39.915	0.7077	0.000004	0.7072
BR8	1174.1	Loves Creek Fm.	18.729	0.7378	0.000009	0.7248
BR9	1170.3	Loves Creek Fm.	133.015	0.7553	0.000008	0.7551
BR11	1163.73	Loves Creek Fm.	21.205	0.7112	0.000007	0.7081
BR13	1157.67	Loves Creek Fm.	55.348	0.7075	0.000003	0.7071
BR15	1151.4	Loves Creek Fm.	61.917	0.7099	0.000004	0.7098
BR16	1149	Loves Creek Fm.	5.333	0.7086	0.000017	0.7077
BR17	1143.3	Loves Creek Fm.	42.897	0.7085	0.000014	0.7078
BR19	1131.8	Loves Creek Fm.	25.198	0.7191	0.000006	0.7152
BR21	1123.9	Loves Creek Fm.	33.316	0.7117	0.000004	0.7090

BR22	1122.7	Loves Creek Fm.	66.366	0.7076	0.000003	0.7072
BR24	1117.6	Loves Creek Fm.	18.534	0.7080	0.000003	0.7074
BR25	1112	Loves Creek Fm.	37.068	0.7168	0.000002	0.7131
BR26	1108.83	Loves Creek Fm.	13.114	0.7096	0.000010	0.7083
BR27	1106.62	Loves Creek Fm.	31.907	0.7110	0.000005	0.7091
BR28	1102.9	Loves Creek Fm.	107.561	0.7077	0.000004	0.7074
BR29	1099.2	Loves Creek Fm.	22.090	0.7086	0.000002	0.7079
BR32	1091.21	Loves Creek Fm.	21.598	0.7086	0.000002	0.7086
BR35	1087.2	Loves Creek Fm.	36.752	0.7122	0.000004	0.7102
BR37	1082.6	Loves Creek Fm.	37.661	0.7100	0.000013	0.7088
BR39	1077.1	Loves Creek Fm.	159.978	0.7069	0.000006	0.7068
BR40	1074.8	Loves Creek Fm.	205.051	0.7084	0.000039	0.7080
BR41	1072.55	Loves Creek Fm.	140.160	0.7089	0.000009	0.7086
BR42	1070.04	Loves Creek Fm.	126.610	0.7074	0.000003	0.7074
BR189	192.5	Ringwood Member	287.682	0.7120	0.000005	0.7114
BR191	189.6	Ringwood Member	183.847	0.7103	0.000003	0.7094
BR193	187.95	Ringwood Member	189.486	0.7102	0.000003	0.7096
BR205	173.6	Ringwood Member	55.498	0.7158	0.000008	0.7126
BR213	164.8	Ringwood Member	31.418	0.7126	0.000006	0.7108
BR216	162.45	Ringwood Member	182.045	0.7112	0.000004	0.7099
BR218	160.15	Ringwood Member	213.309	0.7091	0.000005	0.7085
BR219	159	Ringwood Member	167.034	0.7108	0.000002	0.7097
BR223	155.7	Ringwood Member	167.759	0.7104	0.000005	0.7097
W1	1957.8	Loves Creek Fm.	27.378	.7068	.000003	0.7066

W2	1953.52	Loves Creek Fm.	70.029	.7173	.000005	0.7128
W3	1952.3	Loves Creek Fm.	27.369	.7078	.000005	0.7076
W4	1951.65	Loves Creek Fm.	31.315	.7066	.000006	0.7065
W5	1951.3	Loves Creek Fm.	53.878	.7073	.000004	0.7072
W6	1950.6	Loves Creek Fm.	32.076	.7075	.000005	0.7070
W7	1949.58	Loves Creek Fm.	55.203	.7086	.000002	0.7084
W8	1948.6	Loves Creek Fm.	72.838	.7094	.000002	0.7087
W9	1948.26	Loves Creek Fm.	41.117	.7105	.000009	0.7083
W10	1946.75	Loves Creek Fm.	34.376	.7078	.000004	0.7075
W11	1945	Loves Creek Fm.	198.133	.7081	.000004	0.7074
W12	1944.4	Loves Creek Fm.	110.133	.7101	.000002	0.7085
W13	1942.96	Loves Creek Fm.	227.529	.7091	.000002	0.7082
W14	1941.25	Loves Creek Fm.	276.831	.7095	.000003	0.7090
W15	1940.5	Loves Creek Fm.	122.478	.7108	.000003	0.7098
W16	1938.47	Loves Creek Fm.	60.570	.7295	.000003	0.7185
W17	1936.65	Loves Creek Fm.	62.606	.7136	.000003	0.7107
W18	1933.75	Loves Creek Fm.	285.612	.7073	.000003	0.7071
W19	1932.8	Loves Creek Fm.	100.948	.7119	.000003	0.7097
W20	1930.4	Loves Creek Fm.	305.330	.7071	.000004	0.7069

12. APPENDIX D: GEOCHEMICAL DATA

Major elements

All concentrations in ppm

Sample ID	Mg	Al	Si	K	Ca	Mn	Fe
BR1	63722.424	4465.109	7782.471	2432.340	140723.222	130.052	2947.240
BR2	52670.156	3037.518	2341.930	668.079	86533.184	83.988	1303.529
BR3	45175.579	567.952	4033.367	882.051	80383.930	62.530	1038.038
BR4	103805.094	6620.692	9183.815	5101.389	179088.469	221.424	8762.274
BR5	136825.344	885.313	4029.823	859.081	248443.988	177.541	3276.029
BR6	136982.232	1064.439	8488.904	981.172	238317.406	189.216	3845.145
BR7	8469.341	222.000	756.049	523.823	191356.370	43.045	1530.592
BR8	40078.539	2491.137	7264.044	2423.107	85020.501	84.898	1247.572
BR9	29365.310	463.903	4860.078	255.210	85083.214	42.051	947.430
BR11	66889.097	581.753	3926.635	553.689	118218.163	77.005	1042.215
BR13	131081.321	316.800	372.692	597.041	266644.843	185.182	4984.890
BR15	5653.183	207.048	264.546	498.646	107363.737	185.032	538.094
BR16	10978.548	152.614	<193.20	548.102	19063.855	<21.60	163.642
BR17	129241.984	823.268	1095.509	247.638	269788.436	183.859	1833.586
BR19	81201.370	1156.406	5333.158	1308.274	144388.098	106.088	1269.672
BR21	101294.668	1450.756	2302.902	1609.556	188889.688	170.087	2112.614
BR22	147840.621	407.557	692.978	894.084	273929.557	190.889	1870.604
BR24	23766.298	194.277	1972.668	498.478	45176.611	21.594	367.759
BR25	79299.954	1884.167	2124.143	1304.372	131715.255	83.760	1038.738
BR26	28884.879	229.855	<165.50	622.657	67221.182	33.009	344.571
BR27	137437.603	1232.014	1428.315	762.880	235065.878	174.674	1940.612
BR28	5185.340	457.903	1321.053	252.717	373997.986	58.633	326.697
BR29	27771.218	289.197	268.934	581.018	57100.945	28.853	234.724

BR32	44285.987	4453.715	8452.041	4287.691	69716.311	96.764	2506.369
BR35	113579.844	854.983	1980.816	1149.691	192497.570	226.054	3764.138
BR37	96539.333	615.408	2658.688	344.230	182468.977	188.265	1454.491
BR39	2547.294	338.585	549.036	486.101	269089.317	49.849	200.674
BR40	5878.752	1489.945	1382.586	716.246	291270.764	66.506	742.123
BR41	32286.253	1137.494	1489.972	408.423	87022.520	46.088	1116.962
BR42	9877.927	198.474	980.049	494.053	49709.061	34.637	2102.658
BR189	64972.994	2478.539	2948.519	1633.393	177717.320	2855.296	10332.717
BR191	130670.818	5111.110	6440.223	1912.192	252659.378	3310.837	18002.030
BR193	155006.277	3259.899	4348.970	1519.296	283357.381	3537.345	18067.904
BR205	33979.424	2768.379	5034.956	1990.537	60823.471	972.792	3981.889
BR211	101309.227	6200.626	8807.962	3340.154	181783.606	2933.798	18136.314
BR213	28016.607	1917.514	2480.997	421.994	44655.919	846.764	4151.321
BR216	110791.751	7089.951	7000.397	2063.796	196219.222	2892.776	19045.017
BR218	134468.607	6524.595	7758.061	1653.415	217941.568	2022.630	13936.535
BR219	118712.626	3181.003	6431.787	1488.713	190746.459	1498.494	9008.579
BR223	84368.486	2110.836	3238.167	1195.321	148788.111	882.130	3907.699
W1	1612101	1730.523834	1559.774458	<648.173	3231085.193	2266.035545	25894.29693
W2	1767419.761	81287.65741	117420.8966	35784.413	3404023.885	5270.734424	81079.84263
W3	1095659.013	1956.883988	3901.299526	<711.204	2210465.031	2131.339183	35305.32212
W4	1474967.735	923.4527219	1010.47503	<689.134	2847414.101	2458.410102	16584.56483
W5	1385659.528	1627.915014	1531.313863	<642.043	2751768.99	2165.116132	16910.22606
W6	1497131.097	3949.560222	4454.776677	<883.293	2965106.911	2158.626011	22546.987
W7	1738319.003	4462.679427	12158.87883	1277.220819	3610310.835	2890.088983	47105.61571

W8	1289730.01	24431.87241	61941.40284	5113.05386	2791165.71	3953.019111	316640.0651
W9	1751822.507	36215.76516	45560.17914	6288.535174	3443782.325	3060.131477	48746.11662
W10	1509820.831	4062.177642	3681.16225	<875.902	3429688.483	3009.158973	33383.12815
W11	757824.4134	44284.61428	46296.65243	14862.16538	2095776.692	3100.72845	153248.1531
W12	746233.8552	99798.56854	135209.6889	25985.12885	1658185.01	5076.020563	417850.8079
W13	886115.4351	55933.19497	62850.43006	21674.39898	1940509.863	4144.733032	73981.80879
W14	495093.2294	64096.79369	77097.74507	21684.02596	2219606.097	2903.159227	141213.9018
W15	619769.4304	69086.46234	76389.0381	17001.35652	1354871.268	4792.645201	305157.2427
W16	558749.2995	104984.6605	96889.75493	49390.30017	1022960.084	2559.845818	44659.08432
W17	2008628.567	68268.34498	154635.8201	11048.57264	4062470.055	15415.84905	52437.14917
W18	330580.3212	14936.17646	22704.19767	4113.770987	1922798.648	5291.926091	547898.4348
W19	903562.1621	91181.43074	111188.6081	17603.26456	1862260.323	5999.867819	104443.034
W20	305586.1095	18158.85813	29770.71336	1362.33016	1872213.819	1964.290618	54625.12484

Trace Elements (all concentrations in ppm)

Sample ID	**Rb**	**Sr**	**La**	**Ce**	**Pr**	**Nd**	**Cu**	**P**	**Li**	**Sc**	**Ti**
BR1	9.78	29.62	3.57	8.35	0.95	3.56	6.73	83.46	16.83	1.77	40.40
BR2	3.02	46.07	1.18	2.88	0.30	1.21	1.10	22.33	5.67	0.23	11.69
BR3	2.73	18.96	1.67	3.83	0.41	1.60	0.93	16.90	5.99	0.45	34.14
BR4	18.36	30.54	5.64	13.42	1.62	6.29	5.10	86.59	37.79	4.79	6.67
BR5	1.80	52.02	2.68	6.35	0.75	3.12	44.40	32.84	4.75	1.03	5.79
BR6	2.10	39.34	3.88	9.05	1.04	3.93	9.46	64.63	3.86	0.95	11.19
BR7	0.60	39.91	2.30	3.89	0.41	1.48	0.96	10.19	0.94	0.24	0.96
BR8	7.62	18.73	0.78	1.44	0.17	0.66	3.93	112.25	25.28	1.19	48.40
BR9	0.88	133.01	0.86	1.86	0.23	0.83	4.64	10.45	1.16	0.43	36.15
BR11	2.07	21.21	1.13	2.32	0.27	1.03	2.50	97.76	3.18	0.43	21.48
BR13	0.60	55.35	1.92	4.10	0.48	1.82	3.44	<6.203	2.38	0.79	0.56

BR15	0.30	61.92	1.18	2.81	0.37	1.56	32.52	37.72	1.28	<0.141	0.29
BR16	0.14	5.33	0.12	0.28	0.03	0.13	0.31	11.78	0.22	<0.156	0.90
BR17	0.91	42.90	4.04	7.76	0.85	3.07	9.05	31.03	2.92	0.81	9.98
BR19	3.06	25.20	2.26	4.21	0.50	1.85	11.96	39.59	4.23	0.67	17.07
BR21	2.88	33.32	1.97	4.09	0.49	1.89	1.04	35.73	12.69	0.88	16.82
BR22	0.79	66.37	4.13	7.93	0.90	3.24	11.04	26.18	1.52	0.42	5.75
BR24	0.34	18.53	0.42	0.87	0.10	0.35	0.47	<6.811	0.42	<0.129	3.60
BR25	4.27	37.07	1.09	2.66	0.30	1.21	1.40	38.33	19.46	0.78	17.37
BR26	0.54	13.11	0.83	1.47	0.17	0.66	0.34	14.01	0.65	<0.183	0.56
BR27	1.84	31.91	3.42	7.86	0.98	3.86	0.64	41.59	13.35	1.65	4.01
BR28	1.06	107.56	4.47	7.71	0.84	2.96	0.71	20.03	4.56	0.42	5.11
BR29	0.50	22.09	0.30	0.61	0.07	0.28	0.96	8.52	1.45	<0.139	3.12
BR32	19.26	21.60	2.17	5.24	0.58	2.27	5.03	132.13	87.72	1.44	98.88
BR35	2.26	36.75	1.06	2.17	0.28	1.21	6.54	89.24	12.11	0.40	14.50
BR37	1.30	37.66	1.71	3.90	0.46	1.80	1.45	27.46	4.57	0.29	11.25
BR39	0.26	159.98	1.18	2.01	0.21	0.81	1.57	8.12	2.62	<0.136	1.05
BR40	2.41	205.05	1.23	2.35	0.26	0.94	0.22	58.44	18.76	0.39	6.87
BR41	1.37	140.16	1.12	2.89	0.30	1.26	0.47	36.93	8.13	0.62	7.57
BR42	0.08	126.61	0.15	0.30	0.03	0.13	0.74	<8.903	0.22	<0.169	1.06
BR189	6.76	287.68	6.35	17.24	2.38	12.69	19.07	125.12	15.94	2.63	14.26
BR191	6.22	183.85	8.26	23.03	3.50	16.22	17.12	180.63	10.65	5.45	51.21
BR193	4.35	189.49	4.78	13.67	1.94	8.88	3.22	80.88	7.79	4.14	35.03
BR205	6.99	55.50	4.09	10.87	1.51	6.86	3.23	84.36	13.61	2.77	62.09
BR211	13.67	198.57	8.60	25.26	3.64	16.54	4.29	243.64	21.72	5.29	80.14
BR213	2.19	31.42	3.07	9.52	1.40	6.37	3.71	79.72	6.68	2.93	12.85

BR216	8.78	182.05	11.76	35.80	5.11	23.48	12.14	440.91	17.98	8.15	58.21
BR218	5.22	213.31	8.02	21.88	2.70	10.75	6.65	284.48	15.66	4.59	68.90
BR219	6.72	167.03	6.36	18.14	2.46	10.29	2.50	325.56	17.64	4.18	88.51
BR223	4.50	167.76	3.01	8.25	1.16	4.94	38.34	144.25	11.20	1.70	34.18
W1	0.21	27.38	1.64	3.24	0.34	1.29	0.35	15.63	2.18	0.19	2.59
W2	9.81	70.03	5.64	16.92	2.06	8.28	0.97	10.23	48.46	5.70	11.46
W3	0.17	27.37	1.47	3.60	0.40	1.47	0.50	6.11	0.82	0.20	1.80
W4	0.11	31.31	1.53	3.59	0.34	1.21	0.35	3.47	1.38	0.10	1.04
W5	0.19	53.88	1.27	2.73	0.26	0.96	0.39	5.38	1.34	0.12	2.11
W6	0.53	32.08	2.08	5.50	0.38	1.31	0.26	6.49	2.02	0.43	8.29
W7	0.43	55.20	1.63	3.65	0.39	1.45	1.26	0.51	2.02	0.33	6.11
W8	1.66	72.84	2.13	4.86	0.59	2.19	1.25	1.87	7.95	0.95	7.13
W9	2.84	41.12	3.40	8.19	1.01	3.69	1.80	4.81	13.64	1.58	21.20
W10	0.34	34.38	1.44	3.25	0.38	1.32	0.70	4.73	1.60	0.44	4.89
W11	3.93	198.13	2.44	4.22	0.74	2.95	3.87	7.49	7.81	2.60	12.29
W12	5.30	110.13	3.59	6.55	1.05	4.39	3.27	24.42	9.59	3.83	45.49
W13	6.76	227.53	4.35	9.25	1.31	5.30	2.19	16.43	15.72	4.18	11.83
W14	4.48	276.83	2.18	4.03	0.66	2.68	3.64	23.15	10.78	2.86	17.80
W15	3.86	122.48	2.65	5.23	0.89	3.58	4.65	8.29	6.36	3.51	21.29
W16	20.85	60.57	11.04	25.62	3.54	14.98	1.22	106.93	42.33	9.15	128.65
W17	5.79	62.61	6.18	17.63	1.93	7.63	1.20	13.27	37.49	3.00	23.36
W18	2.10	285.61	1.30	3.16	0.38	1.43	3.06	16.21	1.85	0.92	14.14
W19	6.78	100.95	4.61	11.16	1.29	5.02	1.86	12.94	17.17	5.09	16.67
W20	1.65	305.33	0.79	2.25	0.25	0.96	2.37	1.44	4.39	0.69	2.15